Center for Adhesion Science
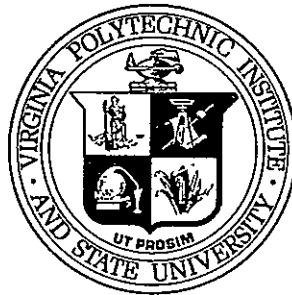
Virginia Polytechnic Institute and State University

Blacksburg, Virginia 24061

FINAL TECHNICAL REPORT

FRACTURE SURFACE ANALYSIS IN COMPOSITE AND
TITANIUM BONDING: PART I. TITANIUM BONDING

BY

K. A. SANDERSON AND J. P. WIGHTMAN

FROM

CHEMISTRY DEPARTMENT

VIRGINIA POLYTECHNIC INSTITUTE & STATE UNIVERSITY

BLACKSBURG, VA 24061

APRIL 1985

ABSTRACT

A CRITICAL STUDY OF THE ROLE OF THE SURFACE OXIDE LAYER
IN TITANIUM BONDING

Methods of joining materials in aircraft structures such as
welding, bolting, and riveting are being replaced by adhesive bonding
because it offers overall weight reduction while maintaining high
strength requirements and superior resistance to environmental attack.
Studies have shown that the surface oxide topography and thickness play
major roles in the bondability on both aluminum and titanium alloys.

The emphasis on the present research is on the analysis of the
interphase, particularly on the analysis of fractured lap shear Ti 6-4
adherends bonded with polyphenyquinoxaline (PPQ) and polysulfone (PS).
The effects of adherend pretreatment, stress level, thermal aging,
anodizing voltage, and modified adhesive of Ti 6-4 adherend bonded with
PPQ on lap shear strength were studied. The largest effect on lap shear
strength can be attributed to adherend pretreatment.

Scanning electron microscopy (SEM) and X-ray photoelectron
spectroscopy (XPS) were used to study the surface topography and surface
composition. Cohesive failure was associated with the absence of a Ti
2p3 XPS photopeak whereas the presence of this peak was evidence of
interfacial failure at the 5 nm level. The Turco pretreated Ti 6-4
cleaned using the grit blast process appeared to give the roughest
surface for bonding in comparison to alkaline peroxide and phosphate-
fluoride surfaces cleaned using the grit blast and Scotch Brite pad
processes. Finally, phosphate-fluoride pretreated Ti 6-4 cleaned by

grit blasting and bonded with polysulfone gave significantly higher lap

shear strengths than a Turco pretreated surface.

TABLE OF CONTENTS

LIST OF TABLES

vi

LIST OF FIGURES

CHAPTER I

INTRODUCTION

Conventional methods of joining materials in aircraft structures such as welding, bolting, and riveting are being replaced by adhesive bonding because it offers overall weight reduction while maintaining high strength requirements and superior resistance to environmental attack. In adhesive bonding, the role of the adherend surface is extremely important and thus it is necessary to develop surface pretreatments which will contribute to stronger and more durable adhesive bonds (1).

Studies (2) on both aluminum and titanium alloy surfaces prepared for adhesive bonding have shown that oxide morphology and thickness play major roles in bondability. Kinloch (3) notes that a surface pretreatment for aluminum alloys based upon phosphoric acid anodization has been developed at the Boeing Aerospace Company. In comparison to the chromic-sulphuric acid etch, the phosphoric acid anodization gives a much thicker and more porous oxide layer as well as a more stable oxide in the hot/wet environment. However, the surface oxide stability of titanium has received considerably less attention compared with the advances being made in the area of adhesives and composite materials (2).

Titanium-to-titanium and titanium-to-composite adhesive bonding is expected to play an important role in the design and production of lighter, high performance air and space crafts of the future. The proposed high operating temperatures, around 300°C, present special

bonding problems since it is required that all bond components, i.e., adhesive, primer, and surface oxide remain stable for long periods at these temperatures (2). There are several titanium alloys that are used in adhesive bonding. However, the most widely used alloy is Ti-(6% Al-4%V). Titanium 6-4 alloy is a highly stabilized alpha-beta phase alloy, using aluminum as the alpha stabilizer and vanadium as the beta stabilizer. These elements impart toughness and strength up to 354°C. Superior in corrosion resistance to many metals, titanium and its alloys are protected by an inherent oxide film at low and moderate temperatures, but are subject to oxidation above 250°C (4). Because of characteristics such as corrosion resistance, high strength to weight ratio, high melting point (1812°C), and the abundance of ore, Ti 6-4 is a material of choice for certain current engineering designs such as high speed aircraft. Consequently, the need to maximize titanium - adhesive bond strength and bond durability has become of great importance.

There is a large market for adhesives as seen in Figure 1. Construction represents the largest share of the market. Furthermore, there are numerous polymer types used as adhesives as shown in Table I. The markets for structural adhesives, in particular, include construction, automotive, aerospace, abrasives, foundry, electronics, furniture, appliances, footwear, product assembly, and other miscellaneous areas. However, there is a need for high temperature structural adhesives where little or no volatiles are produced during processing and which are capable of bonding large areas and providing
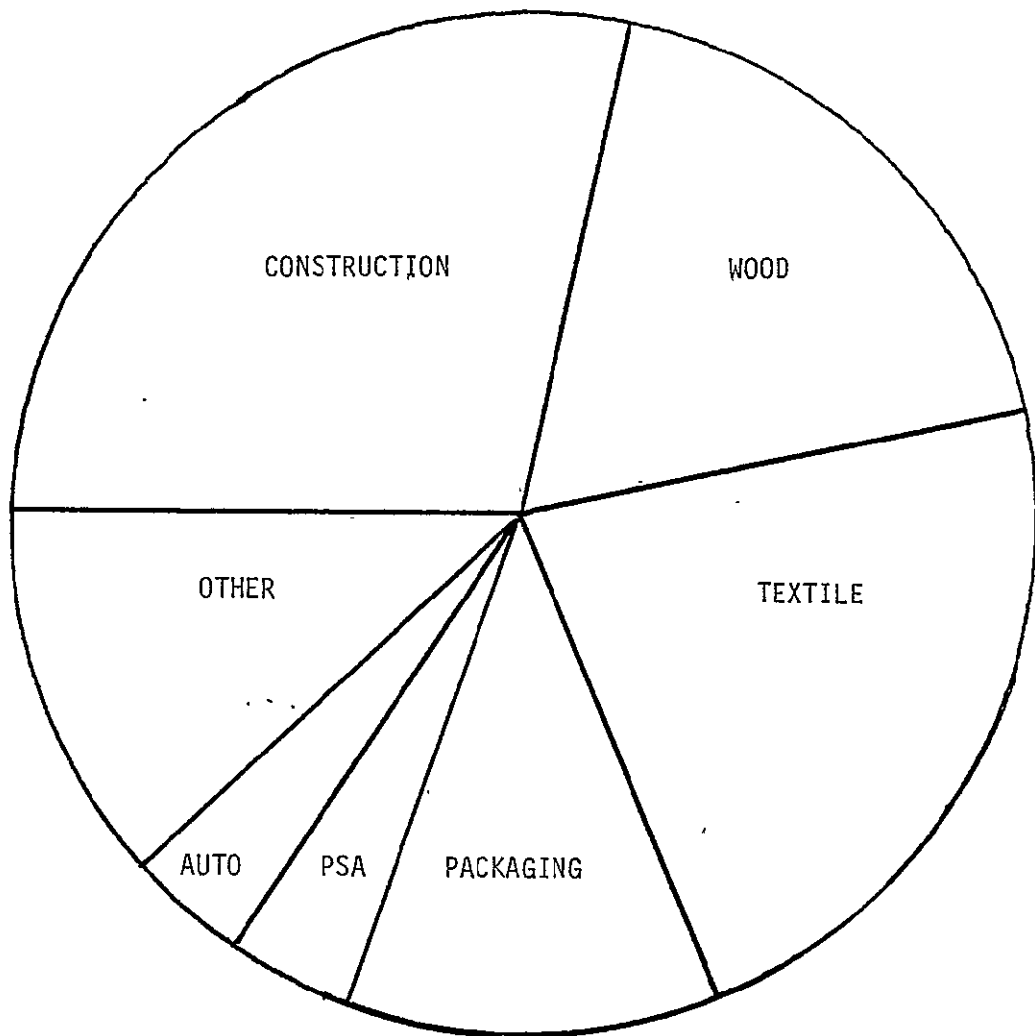
1981 TOTAL 9 BILLION LBS
$3.8 BILLION

Figure 1. Adhesive Markets.

TABLE I

ADHESIVE TYPES

Polymer Type	Markets	%
Thermoplastic	Construction, Textile, Packaging PSA	42
Thermoset	Wood, Auto, Other	28
Elastomer	Construction, Packaging PSA	8
Polysac./Protein	Packaging	13
Other	Construction	9

high strength. The most popular commercially available high temperature
polyimide adhesives that have shown promise in small area bonds for
short terms at 316°C are American Cyanamid's FM-34, Rhodia's Nolimid
A-380, and Dupont's NR150B2G. However, each of these adhesives evolve
considerable amounts (~10%) of volatiles during bonding, which causes
severe problems in bonding large areas (>7.2 cm wide), high porosity in
the bondline, and accordingly, low strengths especially peel strength.
Polyphenylquinoxalines (PPQ) are high-temperature thermoplastic
structural resins synthesized at NASA-Langley Research Center. Although
commercially unavailable, the PPQ's offer an attractive combination of
processing, mechanical, and thermal properties as high temperature
structural adhesives (5). Another multi-purpose thermoplastic of
interest is polysulfone. These sulfur-containing polymers are noted for
their high resistance to temperature , solvents, and chemicals (6). The
polysulfones find great use in areas where the requirements exceed those
available with the lower-cost polycarbonates and aromatic ethers.
Furthermore, the polysulfones have found use in a number of areas
ranging from coffee makers to aircraft and aerospace applications (7).

Hence, adhesive bonding is a multi-faceted system involving
chemistry (synthesis and characterization of polymeric adhesives),
interfaces, and mechanics. The emphasis on the present research.is on
the interphase i.e., the interfacial region between the adherend and the
adhesive. The strength and durability of the adhesive joint are
influenced by many parameters. The choice of adhesive, joint design and
geometry, induced load stresses and environment all affect the bond

strength. Furthermore, the adherend morphology and surface chemistry are all important parameters. Recent studies (2) have shown that the properties of the surface oxide layers on Ti 6-4 may play a key role in the understanding of bond durability. Therefore, the objective of this research is to determine the locus of failure or actually the region of fracture Ti 6-4 specimens bonded with polyphenylquinoxaline and polysulfone by characterizing the fracture surface using SEM (Scanning Electron Microscopy) and XPS (X-ray Photoelectron Spectroscopy).

CHAPTER II

LITERATURE SURVEY

A. Adhesion Concepts

Solid surfaces have a texture which is characterized by waviness, roughness, and indentations such as scratches and pits. Waviness and roughness represent coarsely and finely spaced surface irregularities. They have little effect on adhesive spreading but may affect bond strength if the peaks are sharp edged and act as stress concentration points (8).

Surface indentations may interfere with wetting if they retain trapped air or selectively concentrate solvents from the adhesive. Such air or solvent packets may result in expansion pressure stresses where the bond is cured or used at high temperatures. Schneberger (8) further states that most metal bonding is actually metal-oxide bonding; or more likely, it is metal-oxide, water adsorbed gas bonding. If the oxide is tightly held and cohesively strong, it may provide a better base for bonding than the metal itself. Aluminum is often purposely oxidized (anodized) for this purpose (8).

The concept of wetting refers to the physical affinity between a liquid (adhesive) and a solid (adherend). Thermodynamically, wetting will occur whenever the free energy change producing the liquid-solid interface is negative compared with the free energy changes for loss of the solid-air and liquid-air interfaces (8).

Relating wetting to the work of adhesion involves the relationship between the surface free energies of the surfaces. The thermodynamic

7

work of adhesion, W_A, required to separate unit area of two phases forming an interface may be related by the Dupre equation. In the absence of chemisorption, interdiffusion, and mechanical interlocking, the reversible work of adhesion, W_A, in an inert medium is expressed by equation [1].

$$W_A = \gamma_{SO} + \gamma_{LV} - \gamma_{SL} \qquad [1]$$

γ_{SO} represents the surface free energy of the clean base solid. γ_{LV} represents the surface free energy of a liquid when in equilibrium with its own vapor. γ_{SL} represents the interfacial tension between a solid and liquid. The relationship among the three interfacial energies can also be defined thermodynamically by equation [2].

$$\gamma_{SO} - \pi_e - \gamma_{SL} = \gamma_{LV} \cos \theta \qquad [2]$$

π_e is the spreading pressure of the liquid's vapor on the solid surface and θ is the equilibrium contact angle (9). Therefore, best performance is expected for completely wetted systems exhibiting maximum interfacial contact between materials interacting to give high values of W_A as seen in Figure 2 (9).

Studies by Bowden and Throssel (10) indicate that at room temperature, the adsorbed water layer on metal surfaces is several molecules thick and some water remains even at low humidities. Adhesives therefore should be selected for their ability to spread over and wet highly polar, water rich surfaces (10). Furthermore, bonds are able to resist desorption only if the attaching substances are unable to
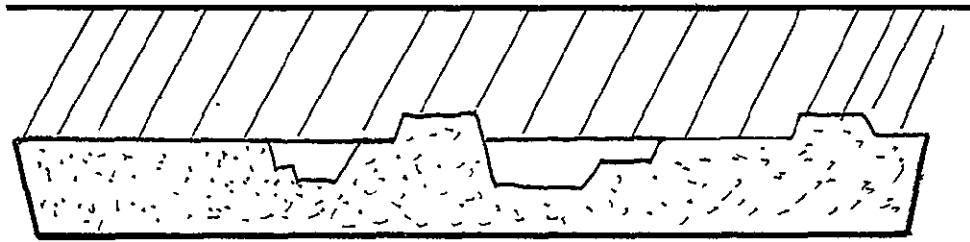
A. Adherend Incompletely Wetted
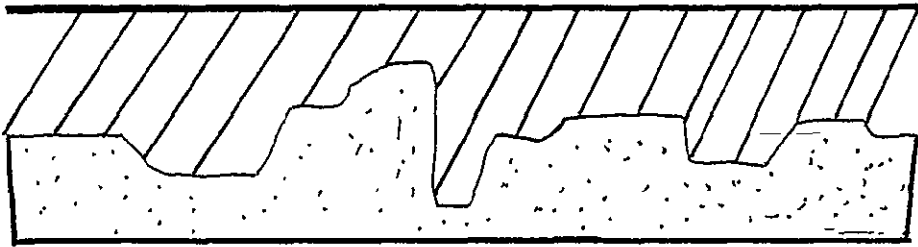
B. Adherend Completely Wetted

Figure 2. Wetting of a Solid Substrate by a Fluid Adhesive.

penetrate the film or if the adherend-adhesive bond is thermodynamically or kinetically favored over the adherend-desorber interaction (8). Of particular importance is the possibility of water penetration at the interface of adhesive and metal. DeLollis (11) comments that if external environment involving water as either liquid or vapor is a problem, thought must be given to using more water-resistant adhesives or primers. The primers must be active enough to desorb or absorb the water and in turn become chemisorbed so that subsequent exposure to an aqueous environment will have minimal effect on bond strength.

The area called the "interphase" plays a major role in understanding the interaction between the oxide/primer and oxide/primer/adhesive interactions. The interphase in most instances is in fact a three-dimensional "interphase" (Figure 3) extending from some point in the adherend where the local properties begin to change from the bulk properties, through the "interphase", and into the adhesive where the local properties again approach the bulk properties. Depending on the actual adhesive-adherend system, this interphase can extend from a few to a few hundred nanometers. On the adherend side, the interphase includes the oxides either deliberately constructed or native to the adherend surface. This oxide can vary in porosity and microstructure from the regular columnar anodized type to natural oxides having a disordered morphology. Adsorbed gases may be present on the oxide surface giving rise to unfavorable thermodynamic wetting of the surface by the adhesive. According to Sanchez (12) classical thermo-

BULK
ADHESIVE

POLYMER
SURFACE LAYER

ADSORBED
MATERIAL

ADHEREND
SURFACE LAYER

BULK ADHEREND
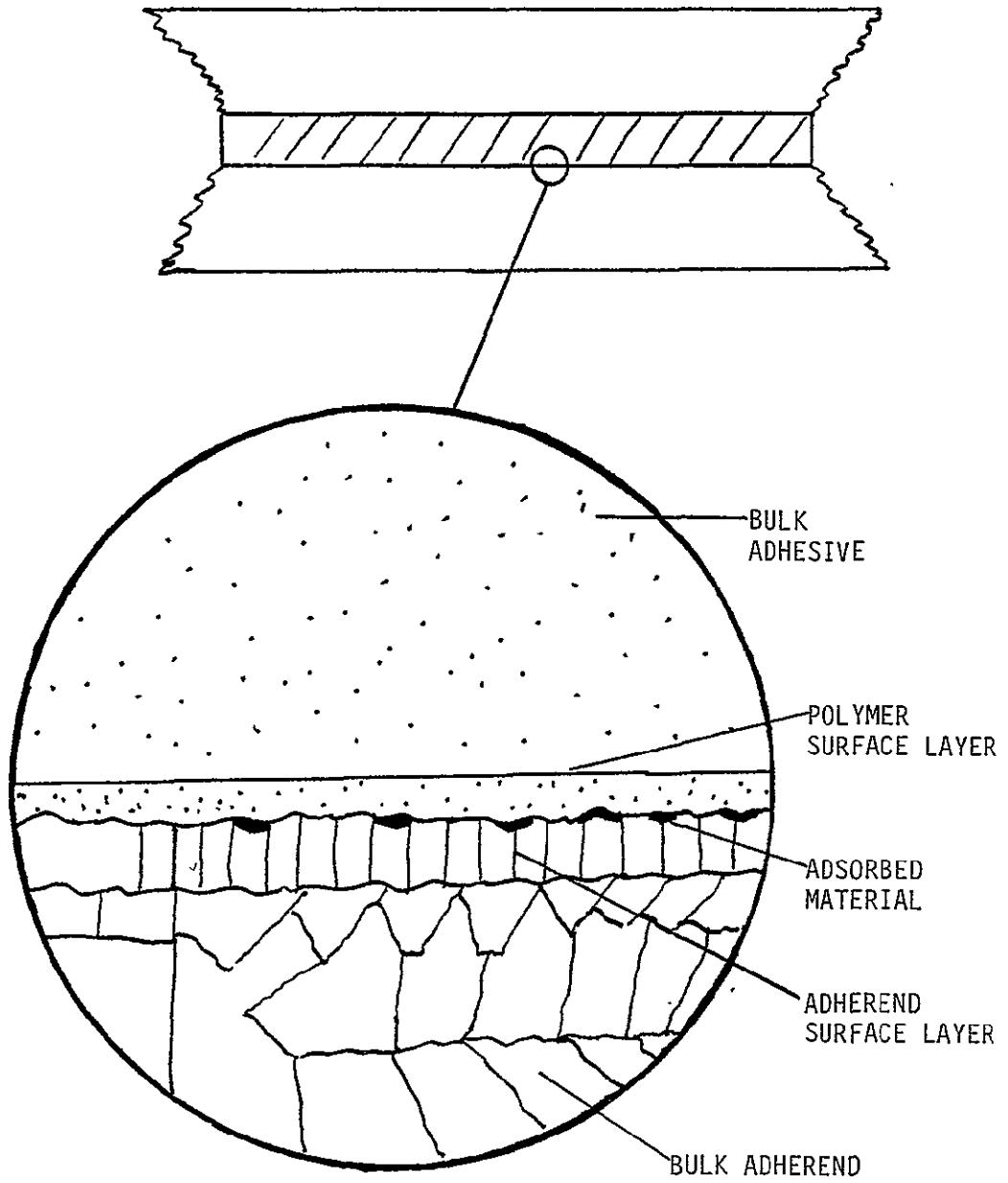
Figure 3. Proposed Three-Dimensional Interphase.

dynamics treats the "interphase" as a "black box." It describes what is in the box, but not how the material is distributed within the box. The power of the thermodynamic description is that it establishes rigorous relationships among the interfacial properties. If an interfacial property is difficult to measure, thermodynamics can suggest alternative properties to measure so that the difficult property of interest can be determined. Furthermore, volatile species may be the source of voids in the formed adhesive bond. The polymeric adhesive is likewise affected by the presence of the adherend surface. Primers used to protect the surface prepared for bonding can create structurally different regions and may contain corrosion inhibiting components present in particulate forms. It is this "interphase" that is formed during the dynamic conditions existing during the processing of the adhesive bond. Therefore, the "interphase" is an integral part of the formed bond and is subject to the mechanical, chemical, and thermal environment seen by the adhesive joint during its useful lifetime (13).

B. Titanium Metals

Various metal adherends such as titanium, aluminum, copper, brass, and stainless steel are used in adhesive bonding. Titanium alloys that can be thermally treated to improve strength, hardness or other properties have attracted the attention of the aerospace industry. Three of these alloys, Ti-17, Ti 10V-2Fe-3Al, and Ti 15-3 can be heat treated by conventional chemical pretreatments. They are basically beta- or "near-beta"-phase alloys that respond to heat treatment by alpha-phase precipitation (14).

Ti- 10V-2Fe-3Al was developed by Timet and is used in several applications on the Boeing 757 and 737-300 aircraft. Forgability and the combination of strength and toughness are reported to exceed those of any other known titanium alloy. Properties include strengthening by a cycle of heating, water quenching, and air cooling; a dynamic modulus of 16,000,000 psi in the aged conditions; and a tensile strength to density ratio of 2.49×10^6 cm at room temperature. It is said to have excellent creep and rupture strength up to 427°C (14).

However, the most widely used titanium alloy is Ti 6-4 which is an alpha-beta alloy (6% Al, 4% V) that is readily available. The beta phase is the high temperature form and exists in equilibrium with the alpha phase at room temperature (15).

C. Pretreatments

It is necessary and common practice to give chemical treatment to titanium alloys before adhesive bonding. One of the main reasons for pretreatment before adhesive bonding is to remove oil and grease contamination (16). An optimized surface for bonding must have a proper balance of roughness and chemistry, not only to ensure high strength bonds, but also ones that have long-term durability under adverse conditions (1). Certain treatments may be used to strip off the natural oxide in preparation for another treatment such as anodization. Other treatments etch the surface to provide favorable mechanical attachment sites of adhesive to adherend. Still others replace the natural oxide with a chemically formed oxide or conversion coating (17-20).

Etching in aqueous hydrofluoric acid or oxidation in alkaline

hydrogen peroxide increases bond strength while etching in acids containing high concentrations of oxidizing agents decrease bond strength when bonded with either modified epoxy, Redux BSL-308, or Hidux 1197C (18). Allen et al. (18) further comment that results indicate that a pretreatment which leaves a coherent TiO_2 rutile layer on a rough surface forms the strongest joints. Furthermore, surface roughness is shown to enhance bond strength. The character of this roughness must be such that the crevices are easily filled by the adhesive flowing without trapping gas bubbles (17).

According to Ditchek et al. (21), results indicate that the ability of the Ti 6-4 adherend oxide to mechanically interlock with an adhesive primer system is the most important factor in determining bond durability. Adherend types can be divided into three groups according to surface roughness produced by different pretreatments. Group I adherends include phosphate-fluoride and modified phosphate-fluoride pretreatments where little or no macroroughness is obtained. A macrorough surface is defined as one having an unevenness with characteristic bumps or jagged edges with dimensions around 1 μm or greater. Microrough surfaces have fine structure with dimensions of 0.1 μm or less. Macroroughness is produced with Group II adherends. Pretreatments in this area include DAPCO treat, dry hone/Pasa-Jell, liquid hone/Pasa-Jell, and Turco 5578. Group III adherends are microporus without macroroughness. Pretreatments in this group include chromic acid anodization and alkaline peroxide (21).

Allen and co-workers (17,18) investigated a number of pretreatment

methods for Ti 6-4 and found that the most effective one e.g., alkaline
hydrogen peroxide, preferentially etched the β phase, gave some
undercutting to the α grains and redeposited needle-like rutile crystals
on the etched β grains. However, according to Ditchek et al. (22), the
porous oxides formed by an alkaline peroxide pretreatment vary
considerably, depending on both temperature, concentration, and
immersion times. Unlike the chromic acid anodized porous oxide, these
oxides have no protruding whiskers to reinforce the bond.

Venables and coworkers (22) have reported results of depth
profiling of the surface oxide layer on Ti 6-4 adherends by Auger
electron spectroscopy (AES). Acidic etches lead to rather thin (20 nm)
oxide layers whereas anodized oxide films are considerably thicker
(40-80 nm). Natan et al. (23) have further reported that initially an
amorphous oxide layer forms on Ti 6-4 adherends pretreated using chromic
acid anodized, alkaline peroxide, phosphate-fluoride, or Turco process.
This amorphous oxide layer in turn can be converted to a crystalline
anatase layer by water immersion at 85°C through a dissolution-
precipitation mechanism. The crystalline layer (beta phase particles),
occupying predominantly ridges and high points on the surface, would be
expected to be the first points of contact for an adhesive material
spread on the surface. Whereas, the steps and ridges of the alpha phase
become important features as etching takes place (15).

The surface titanium oxides produced by different pretreatments can
be amorphous and/or crystalline. Natan et al. (23) comment that
amorphous TiO_2 has been mentioned far less in the literature than the

crystalline polymorphs, possibly because it is identified in a "negative" way, i.e., by the lack of any sharp diffraction patterns. If crystalline TiO_2 is formed, three structures are possible: anatase, brookite or rutile. Anatase has a lower surface energy (24) and a faster rate of formation than rutile. Allen and Alsalim (17) state that no matter which pretreatment is used, rutile is the only crystalline oxide formed on the surface. However, the degee of crystallinity varies for each pretreatment according to selective area diffraction and transmission techniques. Allen and Alsalim found that the crystallinity decreased according to the treatment in the following order judged by the sharpness of the diffraction lines: alkaline hydrogen peroxide, phosphate-fluoride, hydrofluoric acid, anodic anodization, hydrochloric acid, sulphuric acid. Results (21,25) have shown that the chromic acid anodized oxide that precrystallizes to anatase would be an optimum pretreatment for adhesive bonding. It should be further noted that it is generally accepted in adhesion technology, if a freshly pretreated Ti 6-4 surface is not to be bonded within several hours, the surface should be primed for protection. Mason et al. (26) have indeed shown that changes in surface acidity occur on exposure of pretreated Ti 6-4 samples to the laboratory atmosphere.

D. Acid-Base Interactions

It has been suggested that acid-base interactions play an important role in adhesive bonding (27-30). A model for pretreated Ti 6-4 can be developed to account for the surface acidity based on results described by Mason et al. (26). Color changes of indicators spread from solution

on the metal surface were detected using diffuse reflectance visible
spectroscopy (DRVS). Furthermore, Mason et al. used X-ray photoelectron
spectroscopy (XPS) to determine if shifts in binding energy were
observed for the acid and base forms of the indicators on the Ti 6-4
surfaces. It is important to note that both Lewis and Bronsted sites
can interact with the indicators (thymol blue and bromothymol blue) to
change the color. One such pretreatment, phosphate-fluoride, involved
the reaction with HF(aq) and indeed F1s photopeaks were observed with
XPS (20). The Bronsted acidity may be due to the functional groups
shown in Figure 4 (26). The acidity of the surface-OH groups may be due
to the weakening of the OH bond by the inductive effect of the highly
electronegative fluorine (31). Mason et al. (26) found that when the
phosphate-fluoride etched surface was exposed to air, the decrease in
acidity after 10 hours could be due to oxidation of Lewis sites on
adsorption of the basic impurities like NH_3 from laboratory environment.
When the treated metal was heated to 230°C, the acidity decreased
drastically. Removal of water and condensation of adjacent hydroxyl
groups take place at higher temperatures removing Bronsted acid sites as
shown in Reaction [3].
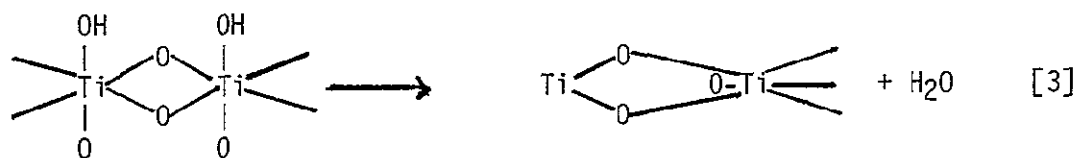
In contrast to the phosphate-fluoride etched surface, the Turco etched
surface is basic. The O⁻ centers formed by Reaction [4], may be the
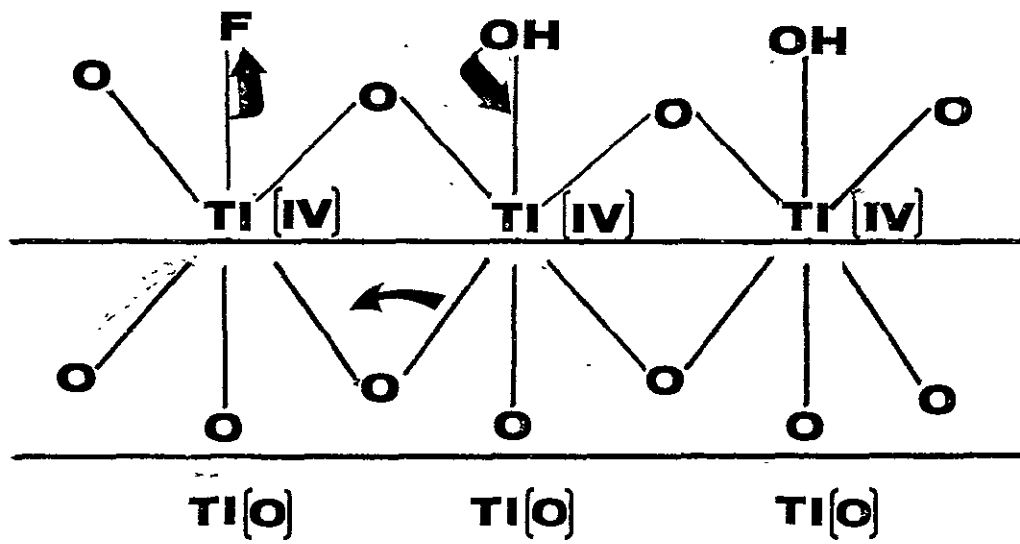
Figure 4. Possible Functional Groups Leading to Bronsted Acidity
of Phosphate-Fluoride Pretreated Ti 6-4 Adherend.

basic sites on the Turco etched surface (26).

$$-M-OH + OH^- \longrightarrow \quad - M(OH)_2^- \rightleftharpoons MO^- + H_2O \qquad [4]$$
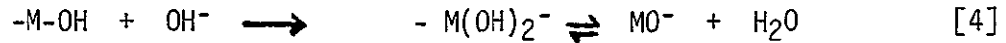
The microstructure of the adherend oxide surface contributes to the adhesive bond by presenting more or less surface area for polymeric/oxide bonding. The degree to which the polymer can penetrate the oxide will influence the mechanical stability of the oxide/polymer bond. The surface chemistry of this adherend oxide influences the degree of chemical bonding between the polymer and oxide. The presence of contaminants on the top oxide surface can interfere with the chemical bond and/or provide a mechanically weak layer at the polymer oxide interface (32).

E. PPQ

Structural adhesives for supersonic cruise aircraft require tens of thousands of cumulative hours of service at temperatures as high as 232°C whereas adhesives and composites for space vehicles must be stable at temperatures as high as 316°C for hundreds of hours. To meet these requirements, a polymer must have a Tg significantly higher than the use temperature. Linear polymers such as polyphenylquinoxaline (PPQ) with high Tgs require processing temperatures approximately 100°C higher than the Tg (glass transition temperature) (33). Small amounts of residual solvent, e.g. 1%, such as m-cresol can serve as a plasticizer to lower the processing temperature but is often undesirable because of venting problems associated with volatiles and/or resultant porosity in the adhesive or composite matrix (33). In fact, it has been suggested that

trace amounts of residual solvent in the bond intensify thermoplastic failure at elevated temperatures (5).

In order to obtain better processibility, Hergenrother (33) has synthesized acetylene-terminated polyphenyquinoxaline (ATPQ) resins. The ATPQ exhibited significantly better processibility than a linear PPQ but the PPQ displayed superior thermo-oxidative stability. However, as the molecular weight of the ATPQ increased, the processibility decreased and the thermo-oxidative stability increased. Hergenrother further notes that the ATPQ resins exhibited good performance as high temperature adhesives for joining Ti-to-Ti and as a resin matrix in graphite filament reinforced laminates. However, in spite of the good performance of the ATPQ resins, the PPQ exhibited better retention of adhesive and laminate properties of 260°C after aging for 500 hours at 260°C in circulating air (33). Hergenrother (34) has also synthesized polyphenylquinoxalines containing phenylethynyl groups. The thermally induced reaction of the phenylethynyl groups provided insoluble crosslinked polymers with high Tg's.

The resin, PPQ, is supplied by NASA Langley Research Center as a monoether polyphenylquinoxaline in a solvent mixture 1:1 of practical grade m-cresol and mixed xylenes formed by the polymer condensation reaction shown in Figure 5.

F. LARC-TPI

Linear aromatic polyimides are presently under consideration for application on future aircraft and spacecraft. Linear polyimides are attractive to the aerospace industry because of their toughness and
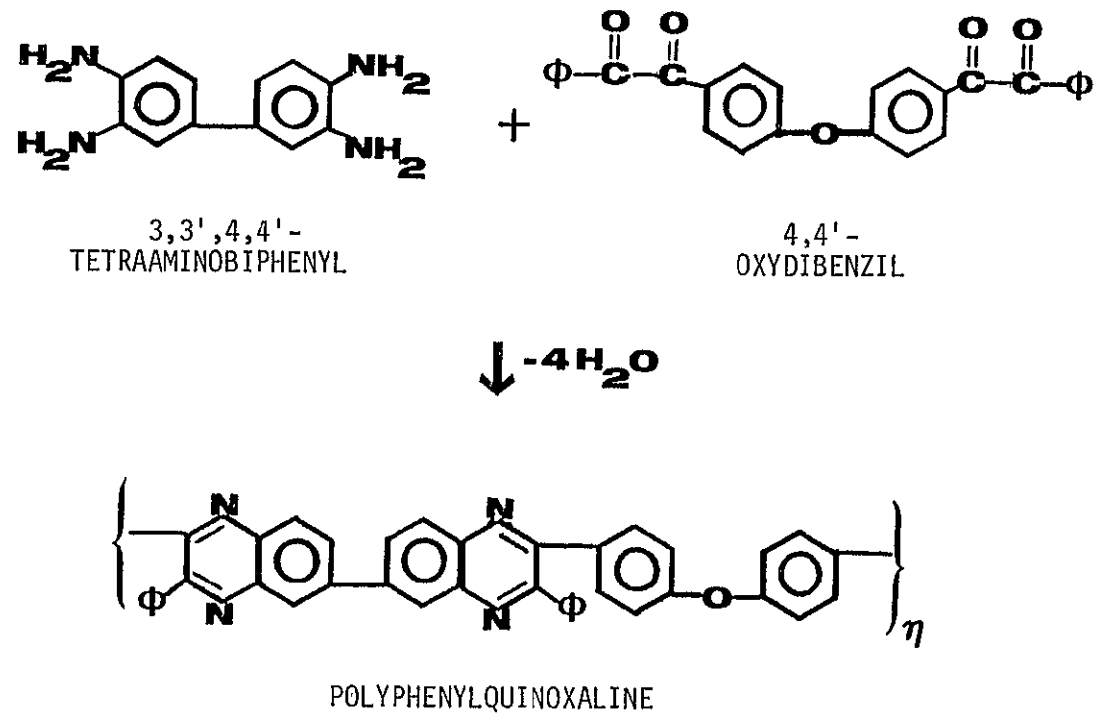
Figure 5.   Polyphenylquinoxaline Synthesis.

flexibility, remarkable thermal and thermo-oxidative stability,
radiation and solvent resistance, lightness of weight, and excellent
mechanical and electrical characteristics over a wide temperature range.
However, the processing of these materials is tedious compared to other
engineering plastics (35).

The use of meta-substituted aromatic diamines in the preparation of
linear polyimides has been a major advancement toward improving the
processibility of these polymers and lowering the glass transition
temperature (35). The adhesive lap shear strength of a meta-oriented
polyimide was improved 2 to 5 fold by synthesis in bis(2-methoxyethyl)-
ether(diglyme) (36,37). More recently this material was used as an
adhesive for bonding ultrathin polyimide film in the proposed NASA-Solar
Sail Program (38).

LARC-TPI is a linear polymer which contains a meta-substituted
diamine and is prepared in an ether solvent. LARC-TPI can be imidized
and freed of volatiles at a reasonably low temperature (230°C) and then
be processed as a thermoplastic. The synthesis follows the reaction
scheme in Figure 6. Because it is processable as a thermoplastic after
imidization and thermally stable at high temperatures, LARC-TPI shows
potential for a variety of applications as listed in Table II (35).

Furthermore, according to St.Clair and St.Clair (35), LARC-TPI is
currently a candidate for the large area bonding of an experimental
graphite composite wing panel in the NASA-Supersonic Cruise Research
(SCR) Program as seen in Figure 7. In addition to being used as an
adhesive, the resin can be precipitated to form a molding powder and

BTDA + M,M'-DABP

15%
DIGLYME
RT

POLYAMIC ACID

$\Delta \downarrow -H_2O$

THERMAL IMIDIZATION

LARC-TPI
THERMOPLASTIC POLYIMIDE
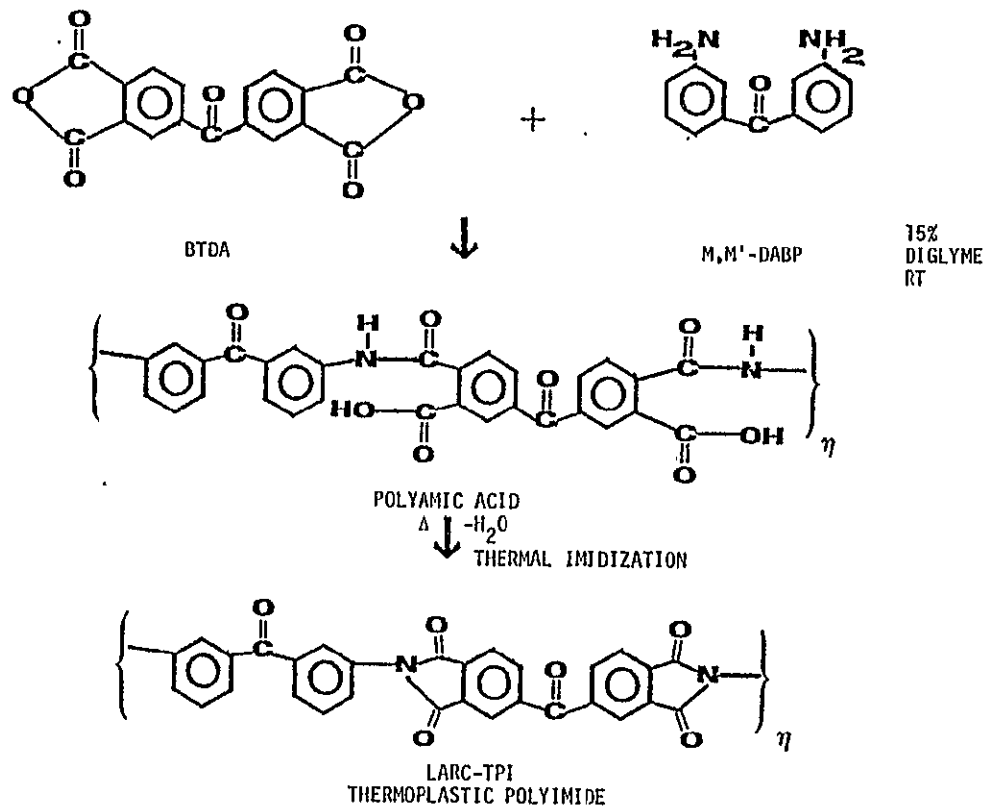
Figure 6. LARC-TPI Synthesis.

DATA FROM	Ti/Ti LAP SHEAR STRENGTH RT MPA(PSI)	Ti/Ti LAP SHEAR STRENGTH 232°C	Ti/Ti LAP SHEAR STRENGTH AFTER 3000h at 232°C Mpa(PSI)
BOEING AEROSPACE	36.5 (5300)	13.1 (1900)	20.7 (3000)
NASA LANGLEY	41.4 (6000)	17.9 (2600)	-
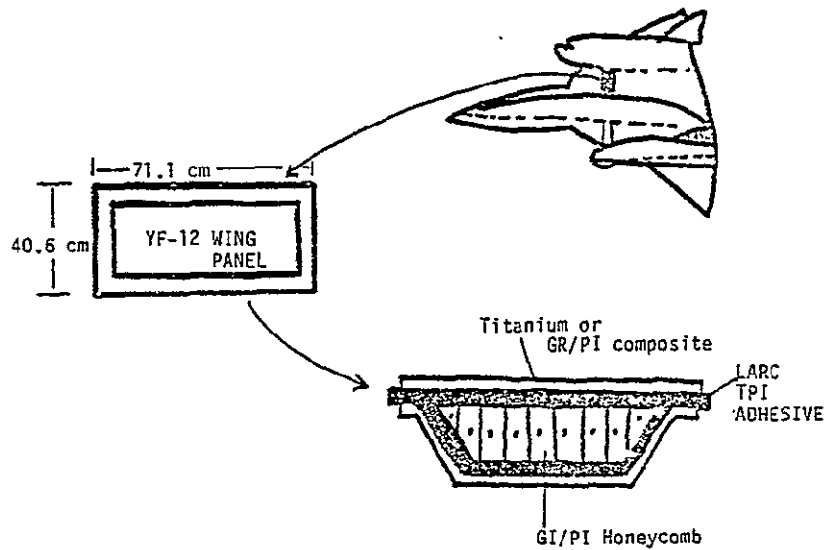
Figure 7. Structural Adhesive Application of LARC-TPI.

TABLE II

APPLICATIONS FOR LARC-TPI

(1) Structural Adhesive for Metals and Composites

(2) Adhesive for Laminating Polyimide Film

(3) Molding Powder

(4) Composite Matrix Resin

(5) High Temperature Film

(6) High Temperature Fiber

thermoplastically molded at 260°C. LARC-TPI also shows potential as a material for making high-temperature films and for spinning high temperature films (35).

G. Polysulfone

The name polysulfone has been assigned to polymers with SO_2 groups in the backbone. At present there are four basic sulfone types: standard, polyaryl, polyether, and polyphenyl. Polysulfone is produced by the reaction between the sodium salt of 2,2-bis(4-hydroxyphenyl) propane (Bisphenol A) and 4,4'-dichlorodiphenyl sulfone as seen in Figure 8 (7).

The unique feature of the chemical structure of these polymers is the diarylsulfone grouping. This is a highly resonating structure in which the sulfone group tends to draw electrons from the phenyl rings. This resonance is enhanced by having oxygen atoms para to the sulfone group. Oxidation, by definition, is a loss of electrons. Schwartz and Goodman (7) comment that having the electrons tied up in resonance imparts excellent oxidation resistance to the polymer. Furthermore, the sulfur atom is in its highest state of oxidation and therefore is not susceptible to further oxidation.

The high degree of resonance has two additional effects: (i) it increases the strength of the bonds involved, and (ii) it fixes this grouping spatially into a planar configuration. This provides excellent thermal stability to the polymer and provides rigidity to the polymer chain, which is retained at high temperatures (7).

The excellent thermal stability of polysulfone is verified by

4-4'-dichlorodiphenyl
sulfone

2,2-bis(4-hydroxyphenyl)
propane

POLYSULFONE

$\eta = 50-80$
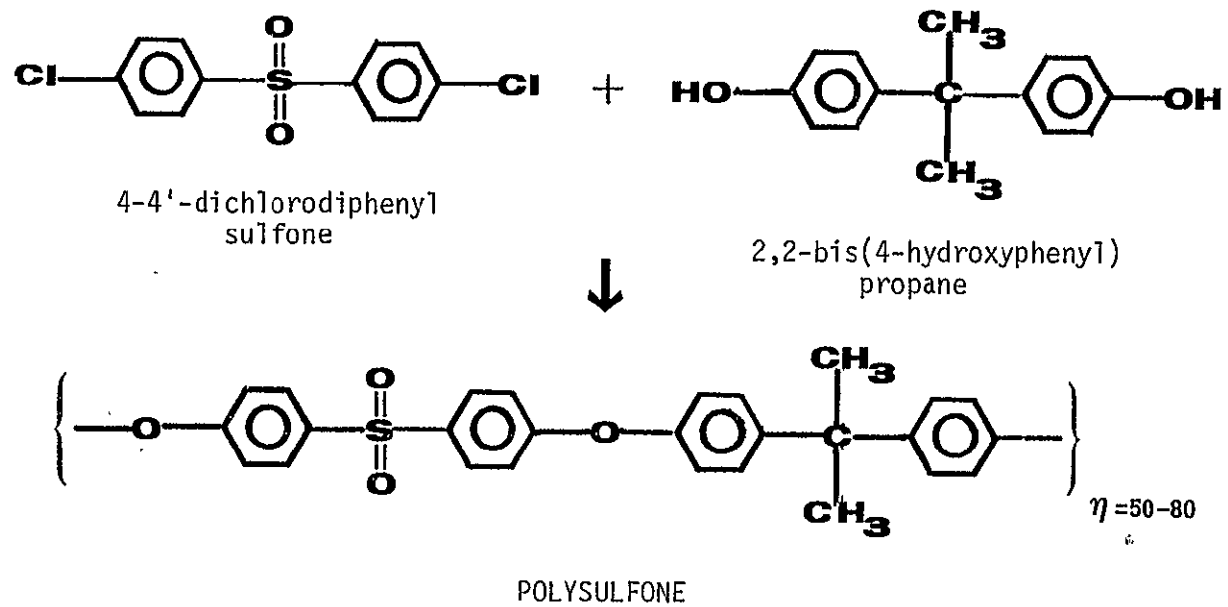
Figure 8. Polysulfone Synthesis.

thermal gravimetric analysis which shows that polysulfone is stable in air up to 450°C. The excellent thermal stability coupled with excellent oxidation resistance of polysulfones provides excellent melt stability for molding and extrusion (7).

Furthermore, the ether linkage imparts some flexibility to the polymer chain which gives inherent toughness to the material. Polysulfone has a second, low temperature glass transition (Tg) at -100°C. This Tg is assigned to the ether linkages.

In these polysulfones, the linkages connecting the benzene rings are hydrolytically stable. Hence, the polymers are resistant to hydrolysis and to aqueous acid and alkaline environments. Schwartz and Goodman (7) noted that this resistance is a distinct advantage over the ester linkages present in polycarbonates and thermoplastic polyesters.

In general, the polysulfones are most noted for their exceptional resistance to creep, good high-temperature resistance, rigidity, transparency, and self-extinguishing characteristics (7).

H. Fracture-Failure Analysis

The theory of attachment sites developed by Lewis and Natarajan (39) states that depending upon the boundary or interphase strength intermediate joint strengths exist and follow the curve of the general form shown in Figure 9.

The model for adhesive joint strength is proposed based on the hypothesis that the strength of the boundary layer is directly proportional to the number of mechanically effective "attachment sites" in the interfacial area between the bulk adhesive and bulk adherend.
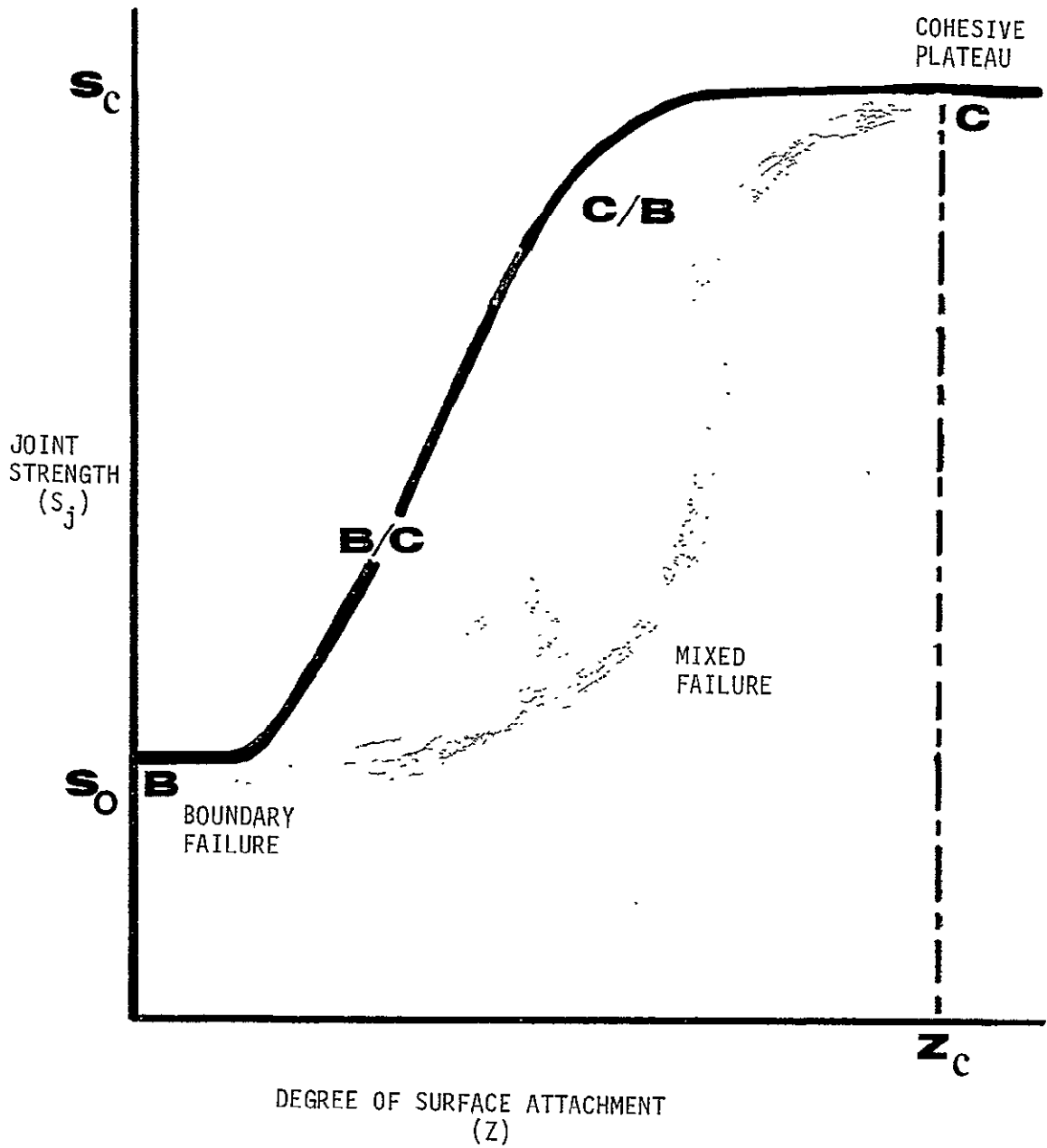
Figure 9. Lewis and Natarajan Theory of Attachment Sites.

Weak boundary layers are characterized by the existence of few or
no operative attachment sites resulting in a low joint strength, S_O,
exhibiting a boundary (adhesive) failure mode. As the number of
effective attachment sites increases by chemical and/or physical
modifications or treatment of the participating surfaces, the joint
strength also increases accompanied by a change to a mixed mode of joint
failure (39).

At a certain saturation level of effective attachment site density,
Z_C, an optimum boundary layer strength is reached where the boundary
layer strength is equal to or greater than the cohesive strength of the
bulk adhesive. Increasing the number of attachments beyond this point
doesn't increase the point strength; the strength of the joint has
reached a so-called "cohesive plateau," S_C. These boundary layer
attachment sites can best be described as being microscopic areas of
attachment at the interface that are capable of contributing to the
mechanical strength of an adhesive joint (39).

The locus of failure in well prepared joints is invariably by
cohesive failure in the adhesive layer. After environmental attack it
is by apparent interfacial failure between the adhesive (or primer) and
the substrate. This interfacial locus of failure means that interfacial
fracture mechanical aspects of adhesive joints become of vital
importance (3). Integral to bond durability is the oxide stability.
Amorphous TiO_2 transformed to anatase TiO_2 under hydrothermal conditions
may decrease bond strength (23). If the amorphous to crystalline
transformation occurred in the adhesive joint, the resulting stress

could promote interfacial failure. To prevent this, the amorphous oxide could be precrystallized to anatase before bonding (40). This would be advantageous since: (i) amorphous oxides have more oxygen vacancies than crystalline oxides (41). Oxygen diffusion from the interface, base metal corrosion, and structural oxide rearrangements are more likely for the amorphous oxide at elevated adhesive joint operational temperatures. (ii) The Ti-O bond for the amorphous oxide is weaker than for the crystalline oxide as confirmed by AES sputtering (40). Dwight et al. (42) found that high temperatures reduce interfacial forces, probably through differential thermal expansion, and the polymer experiences less stress. In other words, without sufficient bonding at the polymer/metal interface, mechanisms that provide adhesive strength (elastic deformation, crazing, etc.) will not come into play. From this point of view, it seems reasonable that overall strength would be the product of an interfacial bonding term and a term that sums the contributors to the strength of the bulk materials (42).

Three commonly used mechanical tests to study an adhesive bond are lap shear test, T-peel test, and crack extension test shown in Figure 10. Two adherend preparations have proven consistently superior for the adhesives studied at the Boeing Aerospace Company (32); namely, chromic acid anodization and phosphoric acid anodization. T-peel specimens have proven to produce low strength values. It was noted by Hill et al. (32) that this is not entirely unexpected since polyimide resins are relatively brittle compared to formulated epoxy adhesives. Consistently lower values in crack length were demonstrated by chromic acid

LENGTH ≈ 305 to 356mm

LENGTH ≈ 152mm
WIDTH ≈ 25.4mm

0.25mm Ti-6Al-4V

1.27mm
Ti-6Al-4V

25.4mm

BONDLINE

203mm

BONDLINE

12.7mm

WEDGE

1.27mm
Ti-6Al-4V

25.4mm

0.25mm Ti-6Al-4V

CRACK EXTENSION (WEDGE)
TEST SPECIMEN

LAP SHEAR TEST SPECIMEN
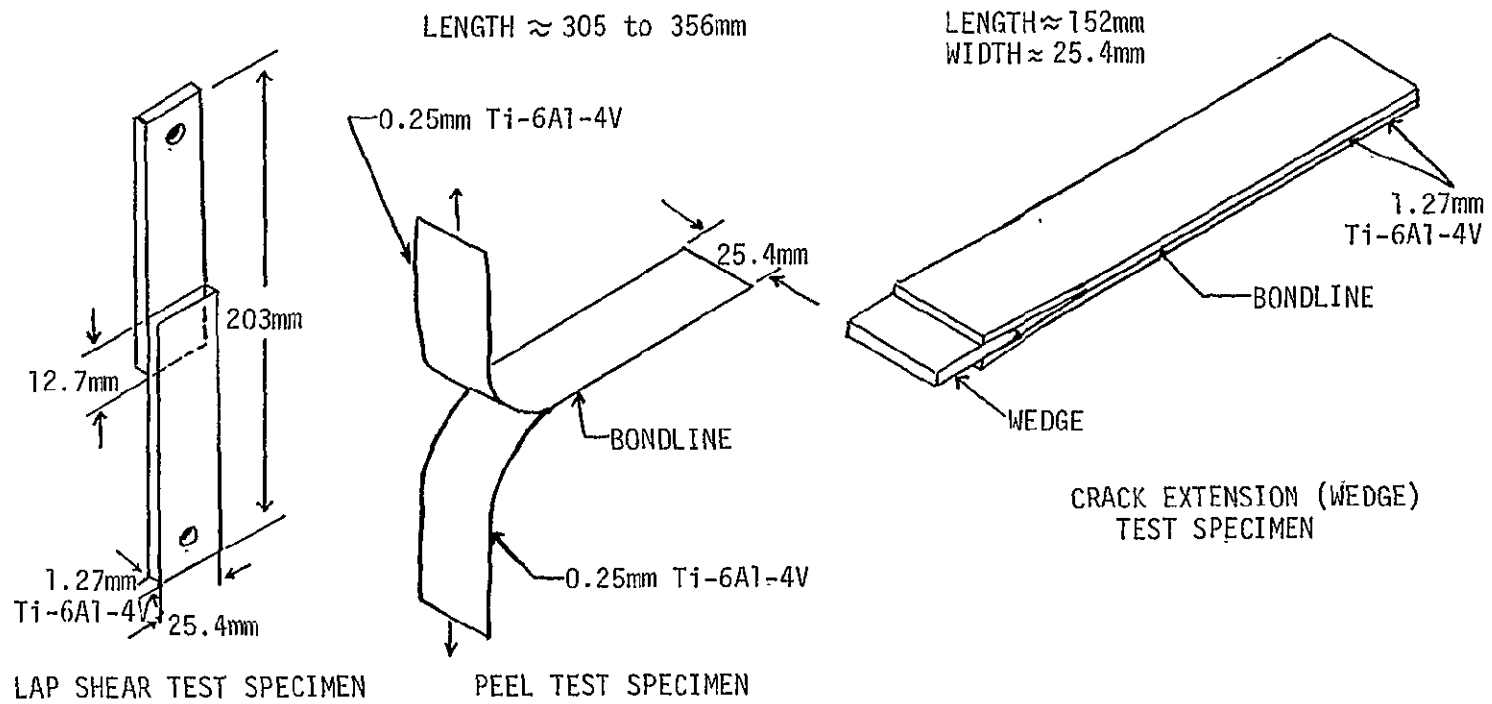
PEEL TEST SPECIMEN

Figure 10. Mechanical Test Specimens.

anodization and phosphoric acid anodization adherend surface treatments compared with other candidate adherend surface treatments (32).

Scanning electron microscopy (SEM) and X-ray photoelectron spectroscopy (XPS) also known as ESCA(Electron Spectroscopy for Chemical Analysis) couple to give a unique "fingerprint" for each particular chemical pretreatment of Ti 6-4 adherends (43). Furthermore, SEM/XPS analysis of fractured surfaces can be used to establish the failure mode. Allen et al. (18) state that techniques such as ion scattering spectroscopy (ISS) and secondary ion mass spectroscopy (SIMS) have been used to provide useful information on the locus of failure in an adhesive joint even when film thicknesses were only on the order of atomic dimensions or where the failure occurs near the original interface and includes parts of both the adhesive and adherend.

SEM is used to evaluate the morphological aspects of bare oxides as well as the interaction of the bonded polymer/oxide. SEM is also used for imaging the bare oxide for gross morphological features such as etch pits or contaminants (32).

The surface chemistry of the adherend oxide influences the degree of chemical bonding between the polymer and oxide. The presence of contaminants on the top oxide surface can interfere with the chemical bond and/or provide a mechanically weak layer at the polymer/oxide interface. Both AES (Auger Electron Spectroscopy) and XPS provide a sensitive way of observing the chemical state of the titanium oxide at the surface and the extent of contamination at the surface. XPS is also used to evaluate the debonded surfaces of the mechanical test specimens

to see if there is chemical segregation at the debonded surfaces, which would contribute to a mechanically weak layer. XPS is also used to determine if the disbond is adhesive or cohesive (32).

CHAPTER III

EXPERIMENTAL

This section contains a description of the materials used and experimental procedures for the various techniques.

A. Samples

Thermally aged fractured lap shear samples were received from the Boeing Aerospace Company as a part of an extensive adhesive bonding program at Boeing under NASA Grant NAS1-15605. Adhesion results obtained in this program have been detailed in a series of reports (44,45). The fractured samples were used as received and are described in Table III. The Ti 6-4 coupons after pretreatment had been bonded with polyphenylquinoxaline (PPQ) or modified polyphenylquinoxaline (PPQ-MI). Five sets of the Boeing samples were analyzed. Set I adherends were pretreated in five different ways, namely by phosphoric acid anodization, Pasa-Jell, phosphate-fluoride (Picatinny), Turco, and phosphate-fluoride (grit blast) processes. Details of the various pretreatments have been given elsewhere (32). Pretreated Ti 6-4 adherends were then bonded with PPQ. Set II adherends were bonded with modified PPQ by the addition of boron powder at 30 phr (parts per hundred resin). The addition of boron modifies the adhesive's coefficient of thermal expansion to more closely match that of the metal adherend. This is desirable for adapting the adhesive system for large area bonding. The Ti 6-4 adherends were pretreated with phosphoric acid anodization, phosphate-fluoride, and Turco processes. The samples in Sets III-V were all pretreated by chromic acid anodization. The aging

TABLE III

DESCRIPTION OF FRACTURED LAP SHEAR SAMPLES BONDED WITH PPQ

Set	Sample No.	Test Temperature	Surface Pretreatment	Lap Shear Strength (psi)	Aging Temp (°C)	Aging Time (hrs)	Stress Level (psi)	Anodizing Voltage(V)	Failure Mode
I	PPQ-B-3	Ambient	Phosphoric Acid Anodized	5120	-	-	-	-	Cohesive
	PPQ-C-5	Ambient	Pasa-Jell	1840	-	-	-	-	Interfacial
	PPQ-E-5	Ambient	Phosphate-fluoride[Picatinny]	2720	-	-	-	-	Mixed
	PPQ-G-3	Ambient	Turco	3100	-	-	-	-	Mixed
	PPQ-H-1	232°C	Phosphate-fluoride [grit blast]	2180	-	-	-	-	Mixed
II	PPQ-M1-E-7	Ambient	Phosphate-Fluoride [Picatinny]	1190	-	-	-	-	Mixed
	PPQ-M1-B-5	Ambient	Phosphoric Acid Anodized	2480	-	-	-	-	Mixed
	PPQ-M1-G-7	Ambient	Turco	1700	-	-	-	-	Mixed
III	117	Ambient	Chromic Acid Anodized	5140	232	500	-	-	Cohesive
	87	Ambient	Chromic Acid Anodized	4790	232	1000	-	-	Cohesive
	336	Ambient	Chromic Acid Anodized	3600	232	2000	-	-	Mixed
	312	Ambient	Chromic Acid Anodized	2640	232	5000	-	-	Mixed
IV	65	-54°C	Chromic Acid Anodized	4390	232	1000	0	-	Cohesive
	239	-54°C	Chromic Acid Anodized	5700	232	1000	1200	-	Cohesive
	284	-54°C	Chromic Acid Anodized	5280	232	1000	1500	-	Cohesive
V	PPQ-5-33	232°C	Chromic Acid Anodized	1500	232	1000	-	5	Mixed
	PPQ-10-33	232°C	Chromic Acid Anodized	2730	232	1000	-	10	Cohesive

time at 232°C of the bonded samples was varied in Set III. Aging times
ranged from 500 to 5000 hours. In Set IV, the stress level of the
bonded samples varied between 0 and 1500 psi. Finally, in Set V, the
anodizing voltage was either 5 or 10 V.

The fractured Ti 6-4 surfaces were categorized by visual inspection
according to the mode of failure as interfacial, cohesive, or mixed
mode (see Table III). If adhesive remains on each adherend and failure
appears to have occurred in the adhesive itself, failure is termed
cohesive failure. If the failure appears to have occurred at the
interface between the adhesive and the adherend, it is termed
interfacial failure (46). Mixed mode failure occurs when adhesive and
metal appear on both adherends. A .95 cm diameter sample was punched
for XPS and SEM analysis after visual examination of the surfaces. The
punched samples were then assigned to one of the following groups:
adhesive failure surface (AFS), metal failure surface (MFS) or fracture
surface (FS). The adhesive failure surface (AFS) of the punched sample
is the surface that contains primarily adhesive in the case of either
interfacial or mixed mode failure. The metal failure surface (MFS)
contains primarily metal in either interfacial or mixed mode failure.
The failure surface (FS) is one that results when there is failure
within the adhesive itself and cohesive failure occurs. These three
failure surfaces are shown schematically in Figure 11.

B. Optical Microscopy (OM)

To obtain an overall view of the samples prior to XPS, AES, and SEM
analysis, a Bausch and Lomb stereozoom optical microscope was used.

ADHESIVE FAILURE SURFACE

TI6-4

METAL FAILURE SURFACE

INTERFACIAL FAILURE

COHESIVE FAILURE

FAILURE SURFACES
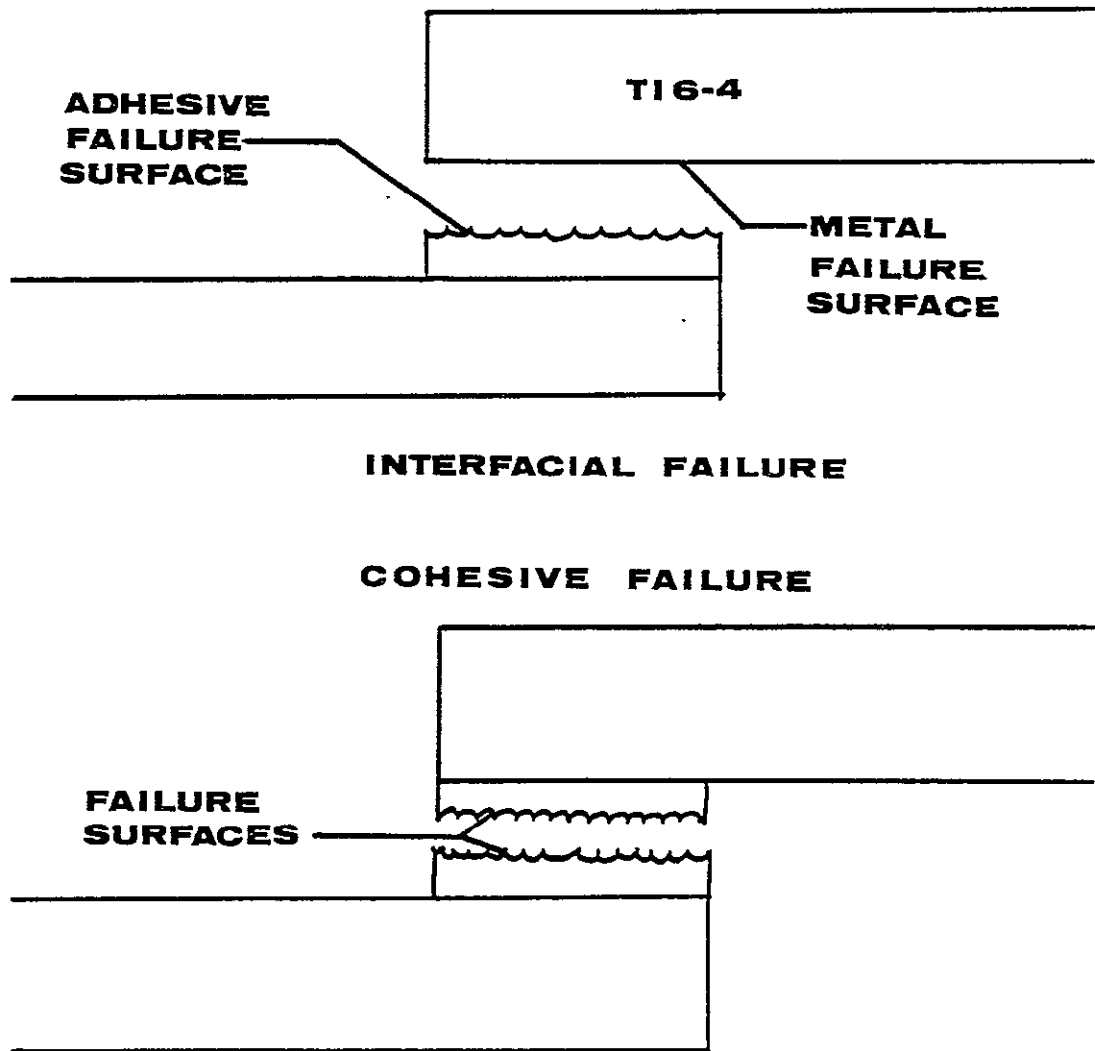
Figure 11. Schematic Diagrams of Fractured Lap Shear Samples.

Photomicrographs of the samples were taken at 10X.

C. Scanning Electron Microscopy (SEM)

All adherends were mounted with copper tape on an aluminum stub. The samples were subsequently coated with gold using a SPI Gold Sputter and photomicrographs at various magnifications were obtained on a JEOL JFM 35c scanning electron microscope.

D. X-ray Photoelectron Spectroscopy (XPS)

The XPS studies were done using two instruments- a Physical Electronics ESCA/SAM 550 electron spectrometer and a Kratos XSAM 800 electron spectrometer. In both cases, a magnesium $K\alpha$ (1.254 keV) anode was used. The data acquisition for the Physical Electronics spectrometer was accomplished using a SAM 550 data system and a Digital PDP-1104 computer. The data acquisition for the Kratos electron spectrometer was accomplished using a DEC-RT-11 computer system. The punched adherends and PPQ powder were mounted with double sided Scotch stick tape. Wide scan spectra (0 to 1000 eV) obtained with the Physical Electronics spectrometer were used to identify major elements present on the surface of the samples. Wide scan spectra obtained with the Kratos spectrometer ranged from 0 to 1200 eV. Major photopeaks were scanned repetitively to obtain the atomic fraction of elements present on the sample surface.

For the Kratos spectrometer, the relative atomic fraction (R.A.F.) of each element was calculated using equation [5].

$$R.A.F. = C.A. * T.F. \div (C.S.*M.F.P.) \qquad [5]$$

The corrected area (C.A.) is equal to the area of a particular. photoelectron peak divided by the number of sweeps. The transmission function (T.F.) is equal to the corrected kinetic energy of the highest peak divided by the corrected kinetic energy of the peak of interest as seen in equation [6].

$$\text{corrected K.E.} = \text{K.E.} + \phi \qquad [6]$$

ϕ is equal to the binding energy correction factor. The product of the photoelectron cross-section (C.S.) times the mean free path (M.F.P.) for each element was obtained from a program written by Glenn Lawson at Virginia Tech. The binding energy of each photopeak is given by equation [7] where $h\nu$ is the incident X-ray energy. The atomic percent (A.P.) for each element was then calculated by equation [8].

$$\text{B.E.} = h\nu\text{-corrected K.E.} \qquad [7]$$

$$\text{A.P.} = \text{R.A.F.}/\sum_i \text{R.A.F.} \qquad [8]$$

E. Auger Electron Spectroscopy (AES)

The AES studies of the fractured samples were done using a Physical Electronics ESCA/SAM 550 electron spectrometer. Data acquisition was accomplished using a SAM 550 data system and a Digital PDP-1104 computer. The punched Boeing samples were mounted with double sided Scotch stick tape. A wide scan (0 to 2200 eV) spectrum was used to identify major elements present on the surface of the samples.

F. Scrim Cloth Aging

Significant amounts of silicon were detected on the Boeing samples. It was speculated that the sizing on the scrim cloth, a glass cloth impregnated with adhesive was degrading either in the bonding or aging process. Therefore, a scrim cloth experiment was designed to study the possible source of silicon.

Four Ti 6-4 coupons were cleaned using a sander. The samples were then cleaned with Scotch brite pads (Al_2O_3 particles) until the surface became smooth and shiny. The coupons were pretreated using the phosphate-fluoride pretreatment described by Hendricks et al. (32). A piece of sized (organosilicon coated) glass scrim cloth (2.5 x 5.0 cm) was placed between two of the coupons. The other two coupons were used as a control pair, i.e., no scrim was used. The samples were then placed in a Blue-M circulating air oven at 250°C. An aluminum bar (39.37 x 5.08 x 1.27 cm) weighing 0.68 kg was used as the weight placed on the two pairs of coupons.

XPS analysis was done following thermal aging for 10 and 100 hours at 250°C for each pair. The samples were thermally aged to determine if the scrim cloth degraded after thermal aging. XPS analysis gave the composition on the surface of the adherend closest to the scrim cloth.

G. PPQ

Due to the occasional detection of lead by XPS in the fractured Boeing samples, subsequent experiments were conducted to aid in finding the source of lead.

Samples of unaged and thermally aged PPQ were analyzed by XPS. The

sample to be thermally aged was placed in a porcelain crucible and covered with aluminum foil. The sample was placed in a Precision Scientific Thelco, Model 16 oven at 190°C for one month.

Finally, a sample of PPQ was analyzed using inductively coupled plasma (ICP). Analysis was done by Ms. Varna at the Naval Air Development Center in Warminster, PA.

H. Pretreatments

To gain a better understanding of the surface morphology and topology of the surface oxide layer, Ti 6-4 coupons were either grit blasted or Scotch brite pad cleaned before pretreatment by Turco (32), phosphate-fluoride (32), and alkaline peroxide (47). The grit blasted coupons were cleaned using a fine size white sand grit applied at an air pressure of approximately 70 psi (pounds per square inch). The Scotch brite pad cleaning process was described earlier. XPS and SEM analysis were done on the treated samples.

An additional Ti 6-4 sample was grit blast cleaned. The sample was phosphate-fluoride pretreated (32) then treated using the Turco process (32). The sample was placed in the Blue M circulating air oven at 250°C for 10 and 100 hours. XPS and SEM analysis were done following the 10 and 100 hours to observe (i) if the silicon was removed by using an acidic pretreatment and (ii) the effect of thermal aging on a Turco pretreated surface.

I. Bonding

Lap shear samples were used to test the adhesive strength of

polysulfone. Four Ti 6-4 coupons were sanded then grit blast cleaned. The cleaned coupons were then pretreated using the Turco or phosphate-fluoride processes. The pretreated coupons were bonded with polysulfone with no more than a 3 hour time lapse between pretreating and bonding.

A 2.54 x 2.54 cm piece of polysulfone film was cut for each pair of coupons. The polysulfone film was prepared in the following manner. Polysulfone pellets were dried in a vacuum oven for 24 hours. For three to four hours of the 24 hour period the pellets were heated at 60°C in a vacuum oven. The dried pellets were stored in a dessicator until ready to cast the film. Two ferrotype plates were cleaned with soap and tap water. The plates were rinsed with tap water then rinsed with methyl ethyl ketone (MEK) and air dried. Four 20 ml shims were cleaned in the same manner. Fifteen to seventeen grams of dried polysulfone pellets were weighed out. One shim was placed at each edge of one of the ferrotype plates. The polysulfone pellets were then placed in the center of the ferrotype plate. The second ferrotype plate was placed on top of the first plate. The two plates were then placed in the press between the two press plates that was heated to 249°C. The plates were preheated without pressure for 2 minutes. After preheating, the pressure was increased to 10,000 psi for 30 seconds then dropped back to 5000 psi. The pressure was then increased to 15,000 psi dynes/cm^2 for 30 seconds then dropped back to 5000 psi. The pressure was increased to 20,000 psi for 30 seconds then dropped back to 5000 psi. The pressure was then increased to 24,000 psi and held for 10 minutes. The plates were cooled under pressure to a press temperature of 170°C. The plates

were removed from the press and the film was popped off with a knife. The film was transparent with no bubbles. The film was wrapped in Kimwipes and aluminum foil until ready to bond.

The lap shear panels were assembled in a jig with a 1.27 cm overlap. The Platen press was preheated to 280°C for 30 minutes. The jig was then placed in the press and preheated with no pressure for 2 minutes. The pressure was increased to 22,000 psi for 10 minutes. The samples were then cooled under pressure to a press temperature of 121°C. The samples were then removed from the jig and wrapped in aluminum foil. The lap shear specimens were then pulled on a Model 1123 Instron at 1 mm/minute to determine the lap shear strengths of the samples. Equation [9] was used to determine the strength of the bonds in units of pounds per square inch (psi).

$$\#kg \times \frac{2.2\ lb}{kg} \times \frac{1}{\text{cross section bonded from fracture surface (sq. in)}} = \#psi \qquad [9]$$

CHAPTER IV

RESULTS AND DISCUSSION

This section contains a description of the experimental results and a discussion of those results.

A. Fractured Boeing Samples

The extent of optical microscopy (OM)/scanning electron microscopy (SEM)/Auger electron spectroscopy (AES)/X-ray photoelectron spectroscopy (XPS) analysis of the Boeing samples is summarized in Table IV. The AES and XPS results obtained on the fracture surfaces are summarized in Tables V-XIII and are discussed below for each sample in Sets I-V.

1. Set I

The Ti 6-4 adherends in Set I were pretreated with five different processes (see Table III) and bonded with PPQ. The effect of different pretreatments on lap shear strength was studied. The AES spectrum for one of the fracture surfaces of Sample No. PPQ-B-3 is shown in Figure 12 and the major peaks are due to carbon and oxygen. The kinetic energy (K.E.) values of the major Auger peaks are listed in Table V. No titanium signal was observed in the Auger spectrum (see Figure 12) consistent with the apparent cohesive failure mode of this sample (see Table V). The XPS results of the fracture surfaces are listed in Table VI. Both fracture surfaces labelled A and B were analyzed by XPS for this sample. The reproducibility of the XPS technique is gauged from the consistency in the values for both the binding energy (B.E.) and the atomic fraction (A.F.) of each observed photopeak on both fracture

TABLE IV

SUMMARY OF WORK DONE ON BOEING Ti 6-4 FRACTURED LAP SHEAR SAMPLES

SET	Sample No.	Technique		
		XPS	SEM	AES
I	PPQ-B-3	X	X	X
	PPQ-C-5	X	X	X
	PPQ-E-5	X	X'	X
	PPQ-G-3	X	X	X
	PPQ-H-1	X	X	X
II	PPQ-M1-E-7	X	X	X
	PPQ-M1-B-5	X	X	
	PPQ-M1-G-7	X	X	X
III	117	X	X	X
	87	X	X	X
	336	X	X	X
	312	X	X	
IV	65	X	X	
	239	X	X	
	.284	X	X	
V	PPQ-5-33	X	X	X
	PPQ-10-33	X	X	
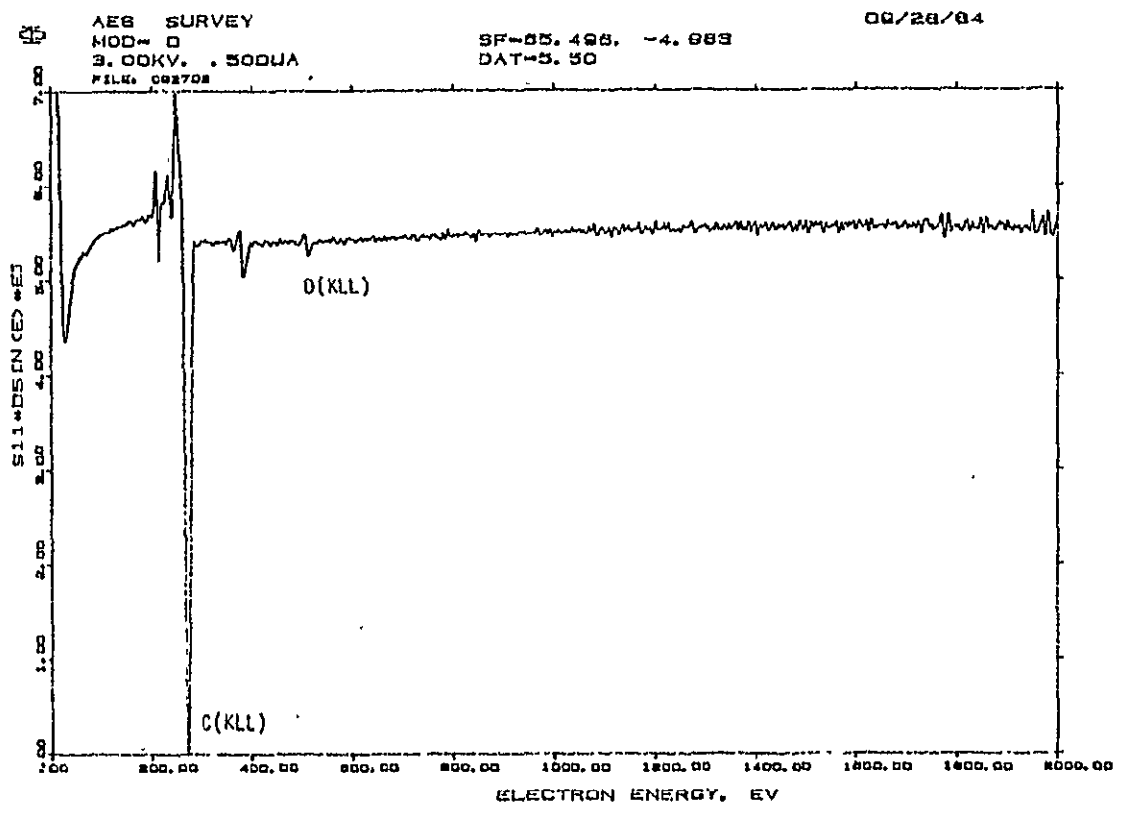
Figure 12. AES Spectrum of One Fracture Surface of Sample No. PPQ-B-3.

47

TABLE V

AES ANALYSIS OF FRACTURED LAP SHEAR SAMPLES
(SET I) BONDED WITH PPQ

PPQ-B-3 (A)		PPQ-C-5(MFS)		PPQ-E-5(MFS)		PPQ-G-3(MFS)		PPQ-H-1(MFS)	
K.E.(eV)	Element	K.E.(eV)	Element	K.E.(eV)	Element	K.E.(eV)	Element	K.E.(eV)	Element
272	C (KLL)	272	C	272	C	272	C	272	C
		382	Ti	382	Ti	382	Ti	382	Ti
		490	0	490	0	490	0	490	0
512	0 (KLL)	512	0	512	0	512	0	512	0

TABLE VI

XPS ANALYSIS OF FRACTURED LAP SHEAR SAMPLES (SET I)
BONDED WITH PPQ

PHOTOPEAK	PPQ-B-3(A)		PPQ-B-3(B)		PPQ-C-5(AFS)		PPQ-C-5(MFS)	
	B.E.	A.F.	B.E.	A.F.	B.E.	A.F.	B.E.	A.F.
F 1s	–	–	–	–	689.2	0.003	NSP	
O 1s	532.0	0.18	532.2	0.14	532.2	0.17	531.8	0.22
Ti 2p3	NSP		NSP		NSP		458.4	0.026
N 1s	398.6	0.021	398.8	0.050	398.8	0.035	399.0	0.025
Ca 2p3	351.6	0.009	NSP		NSP		NSP	
C 1s	285.0	0.76	285.0	0.77	285.0	0.73	285.0	0.65
S 2p	–	–	–	–	168.8	0.010	168.6	0.016
Pb 4f7	–	–	–	–	138.8	0.003	NSP	
Si 2p	102.4	0.032	102.0	0.038	102.2	0.052	102.0	0.063

surfaces. The high binding energy oxygen 1s photopeak at 532.0 eV is attributed to the PPQ adhesive as well as the nitrogen 1s photopeak. The characteristic photopeaks of PPQ are discussed below in Section C. No significant amount of titanium was detected on either surface again consistent with the AES results and hence with fracture in the cohesive mode. The silicon and calcium are most likely due to exposed scrim cloth which is seen in the optical photomicrograph in Figure 13 and more clearly in the SEM photomicrograph in Figure 14.

The AES (see Table V) and XPS (see Table VI) results for Sample No. PPQ-C-5 which apparently failed interfacially are in marked contrast to the results for Sample No. PPQ-B-3 just discussed above. A significant titanium Auger peak is noted in Table V for one of the fracture surfaces which is consistent with the apparent interfacial failure. The detailed XPS results listed in Table VI for the two fracture surfaces indicate significant differences between the two surfaces. The fluorine 1s photopeak is observed on the adhesive failure surface (AFS) but not on the metal failure surface (MFS) which is surprising since fluorine is a residual contaminant on the Ti 6-4 surface following the Pasa-Jell process (32). An oxygen 1s photopeak was observed at approximately 532.0 eV for both the MFS and AFS. If clean interfacial failure had occurred, the oxygen 1s photopeak on the MFS would have been detected at 529-530 eV. Therefore, a residual layer of polymer less than 5 nm thick must be on the metal failure surface shifting the oxygen 1s photopeak to the higher binding energy of 531.8 eV. A significant Ti 2p3 photopeak is observed on the MFS but not on the AFS. This result is interpreted

51

ORIGINAL PAGE IS
OF POOR QUALITY
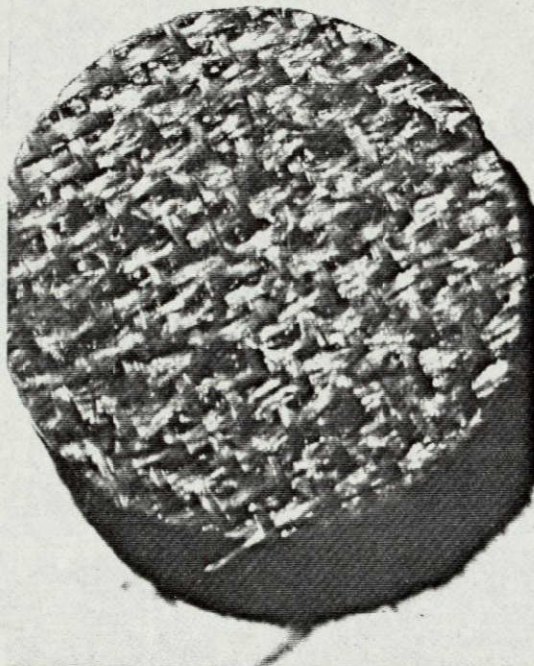
Figure 13. Optical Photomicrograph of One
        Fracture Surface of Sample No.
        PPQ-B-3

52
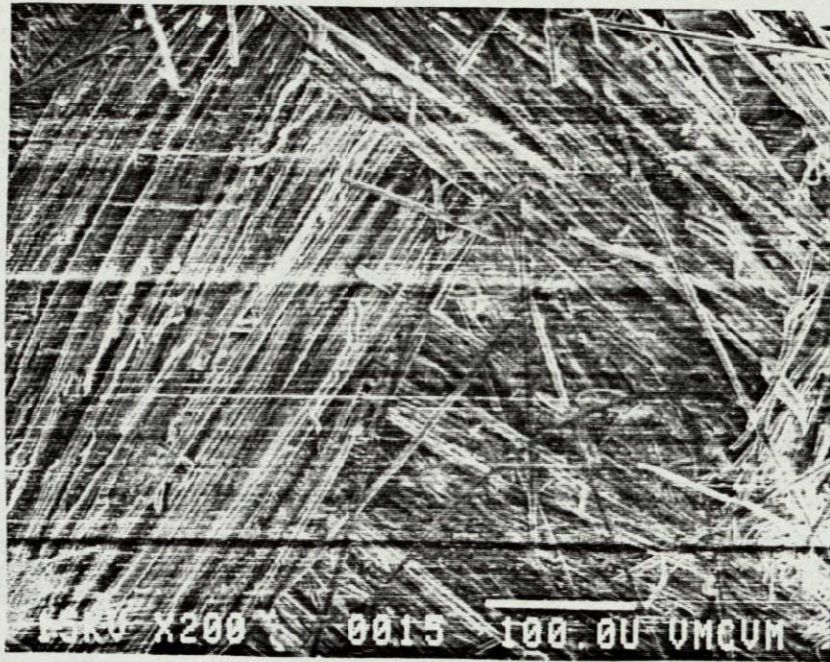
Figure 14. SEM Photomicrograph of One Fracture Surface
of Sample No. PPQ-B-3

to mean that if a residual adhesive film remains on the AFS, its thickness does not exceed 5 nm. Further, with the absence of a Ti photopeak on the AFS, the locus of failure is assigned to the primer/oxide interface rather than within the oxide layer in which case a Ti signal should have been observed on both the AFS and MFS (43). The XPS results for titanium are consistent with the SEM photomicrographs shown in Figure 15; that is, the MFS appears to show areas of exposed Ti 6-4 whereas the AFS appears only to show adhesive. However, such conclusions concerning the locus of failure cannot be based solely on SEM photomicrographs but rather in combination with the surface sensitive XPS technique. The source of sulfur on both fracture surfaces is not known. The presence of lead has been reported previously (32,48). Hill et al. (32) noted that the lead had no significant effect on the bond strengths of the lap shear samples at Boeing. Furthermore, Jen (49) has reported the detection of lead from the XPS analysis of polymer coated glass fibers. It is suggested that solvent(s) used in the synthesis of polyphenyl quinoxaline is the source of the lead. However, the possible effect of lead observed as a trace residual on failure mode remains unanswered.

The AES results for one fracture surface of Sample No. PPQ-E-5 in Table V are similar to those for Sample PPQ-C-5. The XPS results for both fracture surfaces of PPQ-E-5 found in Table VII parallel those for Sample No. PPQ-C-5 except that lead was detected on the MFS rather than the AFS. A minimal titanium photopeak was noted on the AFS as well as on the MFS which supports failure in the mixed mode.
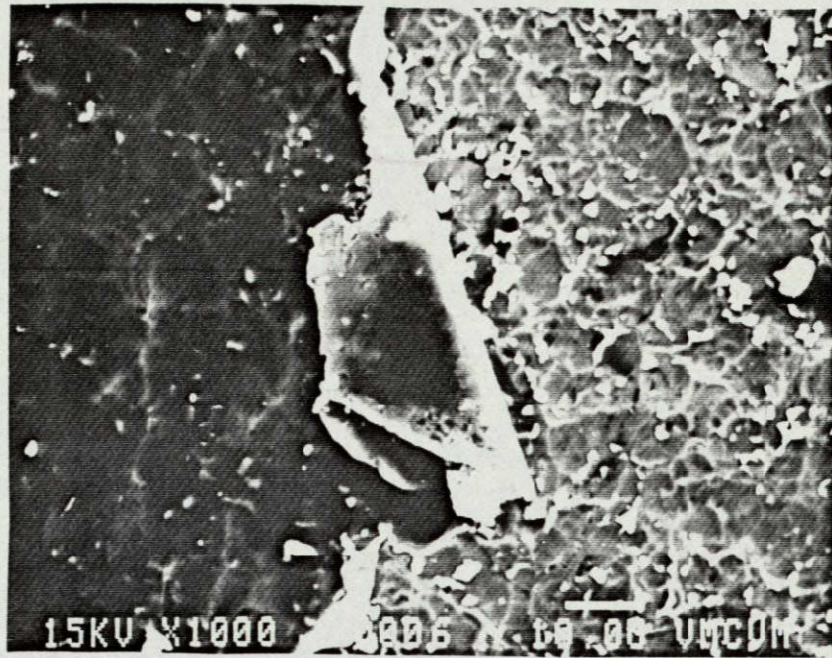
MFS
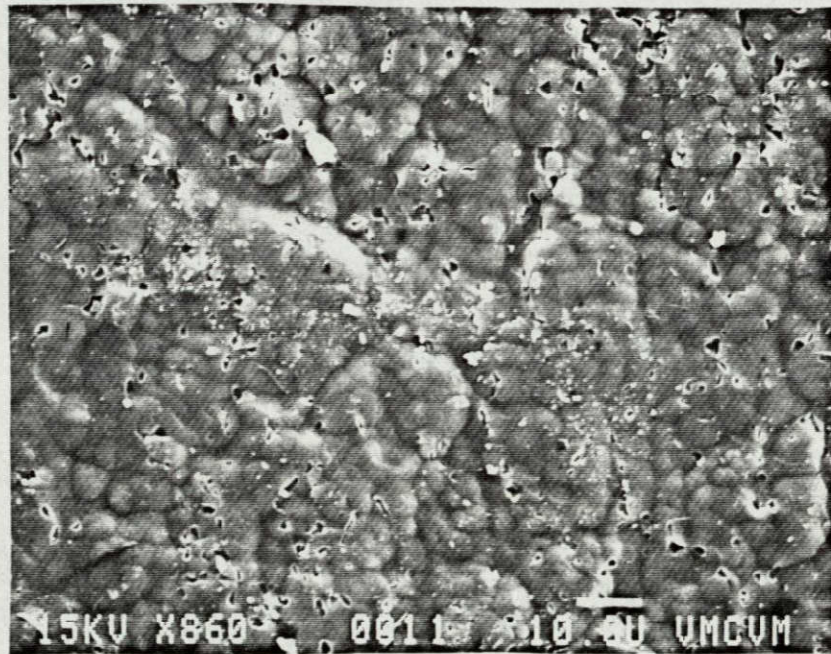
AFS

Figure 15. SEM Photomicrographs of Sample No. PPQ-C-5

56

The AES results for Sample No. PPQ-G-3 in Table V are similar to those for PPQ-C-5 and PPQ-E-5. The XPS results for PPQ-G-3 however differ from those of PPQ-E-5 found in Table VII. A fluorine 1s photo-peak was detected on the AFS of PPQ-E-5 where no fluorine was seen on .PPQ-G-3. The oxygen 1s photopeak at 532.0 eV indicates the presence of PPQ on the fracture surface. No significant titanium photopeak was detected on the AFS whereas a trace amount of titanium was detected on the AFS of PPQ-E-5. A titanium photopeak at 458.4 eV was detected on the MFS of both PPQ-E-5 and PPQ-G-3. Calcium was detected on the AFS of PPQ-G-3 indicative of exposed scrim cloth. Sulfur was detected on the MFS of PPQ-E-5 but not on either adherend of PPQ-G-3. A trace amount of lead was detected on both MFS of PPQ-E-5 and PPQ-G-3. Silicon was detected on both failure surfaces of PPQ-G-3.

The AES results in Table V for one fracture surface of Sample No. PPQ-H-1 are similar to those for PPQ-C-5, PPQ-E-5, and PPQ-G-3. The XPS results in Table VIII indicate the absence of fluorine and sulfur on both fracture surfaces of PPQ-H-1 in comparison with XPS results of PPQ-E-5. The lower binding energy of the oxygen 1s photopeak at 530.8 eV on the MFS is prima facie evidence for a surface titanium oxide layer. Egerton et al. (50) have reported a value of 529.6 eV for the oxygen 1s photopeak in titanium dioxide powder. Furthermore, Filbey (51) has reported oxygen 1s photopeaks for phosphate-fluoride surfaces at approximately 530.6 eV which is further evidence for a surface titanium dioxide layer on the MFS. The oxygen binding energy of 532.2 eV on the AFS is indicative of a polymer coating on the surface however

TABLE VIII

XPS ANALYSIS OF FRACTURED LAP SHEAR SAMPLES (SET I) BONDED WITH PPQ

PHOTOPEAK	PPQ-H-1 (AFS)		PPQ-H-1 (MFS)	
	B.E.	A.F.	B.E.	A.F.
Na 1s	-	-	-	-
O 1s	532.2	0.14	530.8	0.26
Ti 2p3	458.8	0.003	458.2	0.050
N 1s	399.0	0.030	398.8	0.025
Ca 2p3	348.0	0.004	347.2	0.011
C 1s	285.0	0.80	285.0	0.53
S 2p	-	-	-	0.005
Pb 4f7	NSP		138.2	0.005
Si 2p	102.0	0.027	101.6	0.013

not greater than 5 nm. Calcium was reported on both fracture surfaces due possibly to exposed scrim cloth. Lead was detected on the MFS of PPQ-H-1 and not on the AFS.

The variations in lap shear strengths for the samples in Set I are attributed to differences in surface pretreatment. For example, the highest lap shear strength was obtained for phosphoric acid anodized Ti 6-4 whereas the Pasa-Jell process gave rise to the lowest lap shear strength. Hill et al. (32) commented that failure analysis performed on LARC-13 (another structural adhesive) on Pasa-Jell treated adherends suggest failure induced by a lack of chemical cohesion. Furthermore, SEM and STEM (Scanning Transmission Electron Microscopy) analyses demonstrated no gross morphological oxide structure changes occurred and that failure is, for the most part, interfacial to the extent that polymer pull out has even occurred (32). Ditchek et al. (21) also found the absence of Ti on the adhesive failure side of the Pasa-Jell (Group II) pretreated adherend, suggesting that this surface affords the least mechanical interlocking and no micro-roughness as well as exhibiting interfacial failure.

The SEM/AES/XPS analysis of samples in Set I support the different fracture modes. For example, the high lap shear strength samples are associated with cohesive.failure (PPQ-B-3) when no Ti photopeaks were observed in either the AES or XPS spectra.

2. Set II

Set II adherends were pretreated with three different processes (see Table III) and were bonded with modified PPQ. The effect of the

addition of boron to the PPQ on the lap shear strengths was studied.

No AES results for Sample No. PPQ-M1-B-5 were obtained. The XPS results for PPQ-M1-B-5 are found in Table IX. The results indicate the absence of titanium on either fracture surface. However, by simple inspection of the two failure surfaces as seen in the optical photomicrographs in Figure 16, one would classify this fracture as mixed mode failure. Metal visually appears to be present on a part of the MFS but the XPS results show an absence of titanium. A possible explanation is that there is a coating of adhesive greater than 5 nm on the adherend surface. This explanation can be further supported by the high oxygen 1s binding energy of 533.1 eV on the MFS indicative of a polymer (PPQ) coating. This result demonstrates convincingly the power of the XPS technique is defining the locus of failure in adhesive bonding. Trace amounts of fluorine and calcium were observed on the MFS. No boron or lead was detected on either failure surface.

The AES results in Table X for Sample No. PPQ-M1-G-7 are similar to those for Sample No. PPQ-C-5. The XPS results are listed in Table IX. Titanium is only detected on the MFS in contrast to PPQ-M1-B-5 where no titanium was detected on the MFS. A trace amount of sodium was detected on the MFS but not on the AFS. The possible source of residual sodium is from the alkaline peroxide pretreatment. A high oxygen binding energy (~533.2 eV) on both fracture surfaces is indicative of the presence of PPQ on both surfaces. A trace amount of calcium was also seen on the MFS. Again, no boron or lead was seen on either failure surface.

TABLE IX

XPS ANALYSIS OF FRACTURED LAP SHEAR SAMPLES (SET II) BONDED WITH PPQ-M1

PHOTOPEAK	PPQ-M1-B5(AFS)		PPQ-M1-B5(MFS)		PPQ-M1-G7(AFS)		PPQ-M1-G7(MFS)	
	B.E.	A.F.	B.E.	A.F.	B.E.	A.F.	B.E.	A.F.
Na 1s							1073.2	0.004
F 1s			587.1	0.0048				
O 1s	532.5	0.12	533.1	0.12	533.4	0.045	533.2	0.096
Ti 2p3						NSP	459.6	0.004
N 1s	398.0	0.055	398.9	0.042	399.2	0.077	399.2	0.039
Ca 2p3			349.4	0.0043			349.0	0.006
C 1s	285.0	0.79	285.0	0.79	285.0	0.87	285.0	0.84
B 1s						NSP		NSP
Pb 4f7								NSP
Si 2p	102.3	0.019	103.2	0.029	103.4	0.006	103.8	0.008

PHOTOPEAK	PPQ-M1-E7(AFS)		PPQ-M1-E7(MFS)	
	B.E.	A.F.	B.E.	A.F.
F 1s	685.2	0.008		NSP
O 1s	532.4	0.13	530.2	0.17
Ti 2p3	458.8	0.036	459.2	0.018
N 1s	399.2	0.027	399.2	0.037
C 1s	285.0	0.74	285.0	0.77
B 1s	192.4	trace	192.4	0.021
Pb 4f7	138.8	0.001	139.6	NC
P 2P	133.8	0.002	134.6	0.002
Si 2p	102.8	0.012	102.6	0.005

60

61
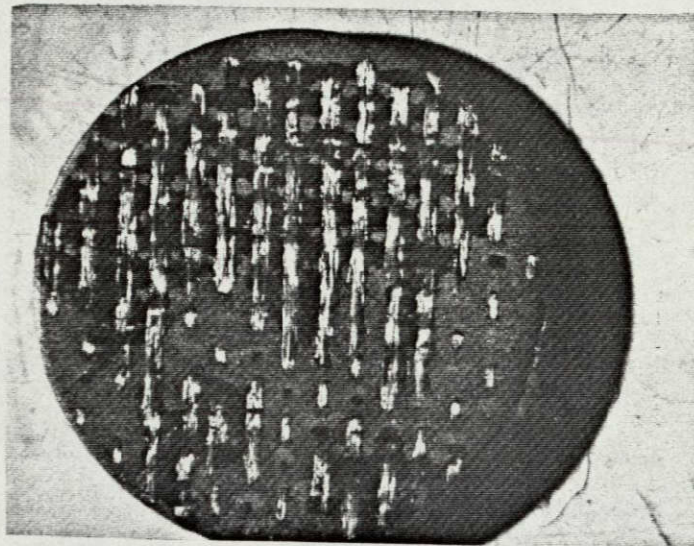
MFS
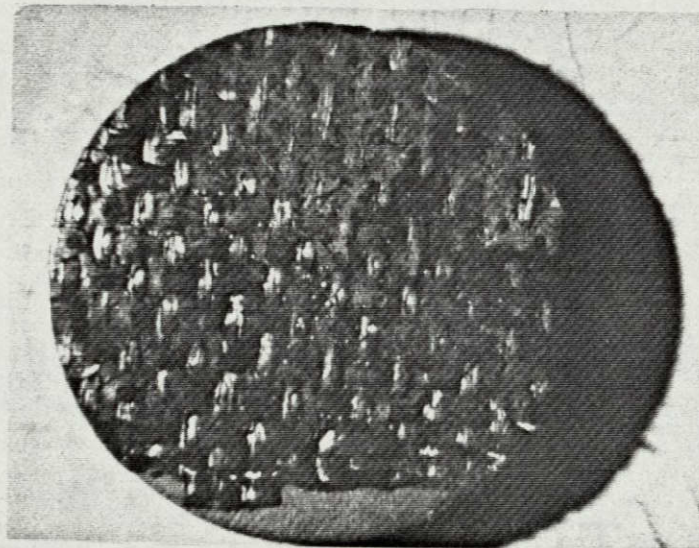
AFS

Figure 16. Optical Photomicrograph of Sample No.
PPQ-M1-B5 Fracture Surfaces

The AES results in Table X for Sample No. PPQ-M1-E-7 are similar to those for Sample No. PPQ-C-5. Titanium is seen on both surfaces supporting mixed mode failure. The XPS results are listed in Table IX. Residual fluorine was seen on the AFS which is surprising since fluorine is a residual from the metal surface pretreatment. Phosphorus was detected on both the AFS and MFS. A possible source of phosphorus is again the phosphate-fluoride pretreatment. Trace quantities of lead were observed again. Boron contained in the PPQ-M1 adhesive was detected on both failure surfaces. A possible answer to why the boron was seen only in this sample is that the boron is not distributed homogeneously throughout the adhesive therefore boron is not always seen by XPS. An oxygen 1s binding energy of 532.4 eV was detected on the AFS indicative of PPQ whereas the 530.2 eV binding energy on the MFS is characteristic of the surface titanium dioxide.

Variations in the lap shear strengths of the samples in Set II are attributed to the modification of the PPQ in combination with different pretreatments. XPS analysis showed no titanium on either fracture surface of PPQ-M1-B-5 therefore failing in the cohesive mode by XPS analysis hence giving the highest lap shear strength. PPQ-M1-E-7 and G-7 failed in the mixed mode giving lower lap shear strengths. Furthermore, the lap shear strengths of Set II were approximately one-half those of Set I pretreated in the same manner. Therefore, the addition of boron powder to PPQ appears to reduce the lap shear strength of Ti 6-4 bonded with the modified adhesive.

The AES results for the remaining sets are all similar to those of

Sample No. PPQ-C-5 except for the detection of sulfur on Sample Nos. 312 and 117. No AES results were obtained for Sample Nos. 87 and PPQ-10-33.

3. Set III

Set III adherends were all chromic acid anodized. The effect of aging time on the lap shear samples was studied.

The XPS results in Table XI for Sample No. 336 surfaces show the presence of titanium on both surfaces supporting mixed mode failure. The oxygen ls photopeak at 532.6 eV is characteristic of the PPQ adhesive however not greater than 5 nm thick. A trace amount of sodium was seen on the MFS. A trace amount of calcium was also detected on the AFS and not the MFS. No fluorine was seen on either failure surface which is in contrast to results that have been reported previously by Ditchek et al. (22). It has been suggested that fluorine is a trace residual from the HF used in the chromic acid anodization.

The XPS results in Table XI for Sample No. 312 surfaces are similar to those of Sample No. 336. The 2.4 eV difference seen between the oxygen ls photopeak on the MFS and AFS is evidence of a clean interfacial failure over at least a part of the fracture surface.

Only one sample for Sample No. 87 was run in XPS due to cohesive failure which is supported by the absence of the titanium photopeak. The XPS results in Table XI are similar to Sample No. 336 except for the absence of titanium in Sample No. 87.

Again, only one sample for Sample No. 117 was run due to failure in the cohesive mode. Titanium was detected in the AES spectra whereas no titanium was detected by XPS (see Table XI). A trace amount of fluorine

TABLE XI

XPS ANALYSIS OF FRACTURED LAP SHEAR SAMPLES (SET III) BONDED WITH PPQ

PHOTOPEAK	336 (AFS)		336 (MFS)		312 (AFS)		312 (MFS)	
	B.E.	A.F.	B.E.	A.F.	B.E.	A.F.	B.E.	A.F.
Na 1s		NSP	1072.4	trace				
F 1s		NSP		NSP		NSP		NSP
O 1s	532.6	0.13	532.6	0.13	533.2	0.12	530.8	0.19
Ti 2p3	459.4	0.007	459.0	0.007	459.2	0.003	459.0	0.041
N 1s	399.2	0.037	399.0	0.04	399.2	0.061	399.4	0.042
Ca 2p3	348.6	0.004			348.8	0.007		
C 1s	285.0	0.79	285.0	0.80	285.0	0.80	285.0	0.72
Si 2p	103.2	0.027	102.8	0.015	104.0	0.007	102.2	0.012

PHOTOPEAK	87		117	
	B.E.	A.F.	B.E.	A.F.
Na 1s	1072.6	trace		NSP
F 1s		NSP	689.4	0.007
O 1s	533.0	0.14	532.8	0.128
Ti 2p3		NSP		NSP
N 1s	399.0	0.053	399.0	0.037
Ca 2p3	348.4	0.007	348.2	0.007
C 1s	285.0	0.75	285.0	0.80
Si 2p	103.6	0.026	103.2	0.032

was detected on the failure surface. No sodium was seen on the failure surface.

In Set III, the effect of aging time of samples aged at 232°C on lap shear strength was studied. Sample No. 117 which had the highest lap shear strength (5140 psi) was aged the shortest time. Furthermore, no XPS titanium photopeak was seen ruling out interfacial failure in this sample. On the other hand, Sample No. 312 had the lowest lap shear strength for the longest aging time as well as giving good evidence from XPS for interfacial failure. Therefore, it appears that the longer the aging time the lower the lap shear strength for adhesive bonds made with PPQ. The aging process at 232°C possibly could be weakening the primer/oxide interface resulting in weaker primer/oxide bonds.

4. Set IV

The samples in Set IV were again all chromic and anodized and aged at 232°C for 1000 hours. However, the variable in this set was the applied stress level.

The XPS results for one fracture surface of Sample No. 284 are found in Table XII. The results are similar to those for Sample No. PPQ-B-3. Only one sample was analyzed due to failure in the cohesive mode. This is supported by the absence of a titanium XPS photopeak and an oxygen 1s photopeak occurring at 532.6 eV.

The XPS results in Table XII for Sample No. 239 resemble those of Sample No. 284 with the exception of the absence of calcium. Furthermore, the XPS results in Table XI for Sample No. 65 are similar to those of Sample No. 239.

TABLE XII

XPS ANALYSIS OF FRACTURED LAP SHEAR SAMPLES (SET IV)
BONDED WITH PPQ

PHOTOPEAK	284 B.E.	A.F.	239 B.E.	A.F.	65 B.E.	A.F.
O 1s	532.6	0.15	532.3	0.15	532.4	0.14
Ti 2p3		NSP		NSP		NSP
N 1s	398.6	0.027	398.0	0.023	398.5	0.029
Ca 2p3	348.3	0.0059				
C 1s	285.0	0.77	285.0	0.78	285.0	0.80
Si 2p	102.7	0.039	102.4	0.037	102.5	0.03

In Set IV, the effect of stress level on lap shear samples aged at 232°C was studied. All three samples showed high lap shear strengths (>4000 psi) characteristic of cohesive failure. This is confirmed by the absence of a Ti XPS photopeak on any of the fracture surfaces. Hence, the variation in stress level on samples aged at 232°C for 1000 hours had little or no effect on lap shear samples pretreated using chromic acid anodization, bonded with PPQ, and tested at 18°C.

5. Set V

Set V samples were chromic acid anodized but at different voltages, 5 and 10 V. The XPS results for both fracture surfaces of Sample No. PPQ-5-33 are found in Table XIII. The results support some interfacial failure due to a minimal titanium signal on the MFS. A trace residual of fluorine (0.5%) was detected on the MFS as was a trace of sulfur. Mandry and Rosenblatt (52) showed that even at very small concentrations (10^{-3} molar) fluorides can result in dissolution of titanium oxide. Thus, Ti adherends that are contaminated with fluorine may fail prematurely in the presence of high humidity conditions. Initial studies on the effects of fluoride ions on Ti 6-4 adherends show that they are not as susceptible to fluorine etching as aluminum adherends, but that fluorine can slowly erode the Ti 6-4 surface (22). The high oxygen 1s binding energy for both failure surfaces was approximately 533.0eV indicative of a polymer coating. Sample No. PPQ-5-33 appeared to be of the mixed mode failure however by XPS it appear to be mainly cohesive failure. No lead was detected on either failure surface.

XPS results for one of the fracture surfaces of Sample No.

TABLE XIII

XPS ANALYSIS OF FRACTURED LAP SHEAR SAMPLES (SET V)
BONDED WITH PPQ

PHOTOPEAK	PPQ-5-33 (AFS)		PPQ-5-33-(MFS)		PPQ-10-33	
	B.E.	A.F.	B.E.	A.F.	B.E.	A.F.
Na 1s					1071.8	0.003
F 1s		NSP	689.6	0.005	689.6	0.004
O 1S	533.0	0.13	532.8	0.11	532.6	0.14
Ti 2p3			459.4	0.001		NSP
N 1s	399.2	0.053	399.4	0.046	399.4	0.032
Ca 2p3					348.2	0.007
C 1s	285.0	0.80	285.0	0.82	285.0	0.74
S 2p			168.2	0.006		
Si 2p	103.6	0.02	102.2	0.014	103.0	0.026

PPQ-10-33 are found in Table XIII. XPS supports failure in the cohesive mode as shown by the absence of a titanium XPS photopeak. Fluorine, calcium, and sodium were detected on the failure surface.

In Set V, the effect of anodizing voltage on lap shear samples aged at 232°C was studied. The spectroscopic evidence is not as definitive as in the other four cases above but a weak titanium XPS photopeak was observed on the 5V anodized Ti 6-4 adherend which gave the much reduced lap shear strength. Therefore, according to the results obtained, chromic acid anodization at 10V gives superior lap shear strengths to those obtained with 5V anodization.

B. Scrim Cloth Aging

Due to the occasional detection of silicon on the Boeing fracture surfaces, a scrim cloth experiment was designed to determine if the source of silicon was due to the thermally aging and subsequent degradation of the scrim cloth sizing. The XPS results are listed in Tables XIV and XV. Both adherends, labelled top and bottom were analyzed for the control and scrim cloth pairs. The reproducibility of the XPS technique is gauged from the consistency in both the binding energy (B.E.) and in the atomic fraction (A.F.) of each observed photopeak.

The binding energy of about 530 eV for the oxygen 1s photopeak remains constant for the control pair. The average binding energy of 530.4 V is consistent with results of Wightman (43) and arises from the surface oxide layer. Similarly, the titanium 2p3 photopeak, assigned to the tetravalent state of titanium and present as titanium dioxide (TiO_2)

TABLE XIV

XPS RESULTS OF SCRIM CLOTH AGING

PHOTOPEAK	CONTROL 10h(TOP)		CONTROL 10h(BOTT)		CONTROL 100h(TOP)		CONTROL 100h(BOTT)	
	B.E.	A.F.	B.E.	A.F.	B.E.	A.F.	B.E.	A.F.
O 1s	530.1	0.37	530.9	0.37	530.3	0.46	530.2	0.36
Ti 2p3	458.7	0.12	458.5	0.13	458.9	0.10	458.7	0.11
C 1s	285.0	0.41	285.0	0.38	285.0	0.34	285.0	0.42
P 2p	-	-	-	-	133.4	0.006	133.1	0.017
Al 2p	78.8	0.019	74.8	0.025	73.8	0.022	74.1	0.019
Si 2p	trace		-	-	-	-	-	-

71

TABLE XV

XPS RESULTS OF SCRIM CLOTH AGING

PHOTOPEAK	SCRIM 10h(TOP) B.E.	A.F.	SCRIM 10h(BOTT) B.E.	A.F.	SCRIM 100h(TOP) B.E.	A.F.	SCRIM 100h(BOTT) B.E.	A.F.
O 1s	529.7	0.36	530.8	0.37	529.9	0.39	530.3	0.36
Ti 2p3	458.2	0.12	458.4	0.13	458.7	0.12	458.8	0.086
N 1s	399.6	0.0085	-	-	-	-	-	-
C 1s	285.0	0.42	285.0	0.40	285.0	0.39	285.0	0.45
Al 2p	73.5	0.021	73.8	0.023	74.0	0.023	74.1	0.022

is constant at about 458.5 eV (43). Phosphorus was detected on the 100 hours aged sample but not the 10 hours aged samples. The detection of phosphorus is a result of trace residuals from the phosphate-fluoride pretreatment. Aluminum was detected on all adherends. Possible sources are (i) migration of aluminum from within the alloy, (ii) contamination from the aluminum sheet the coupons were placed on in the oven, or (iii) residual embedded aluminum from the Scotch brite pad cleaning. Only a trace amount of silicon was see on the control sample (TOP) at 10 hours. No silicon was seen on the remaining control adherends.

The oxygen binding energy of the scrim cloth pair at 10 and 100 hours was approximately 530 eV. The titanium binding energy for the 10 and 100 hours samples was on the average of 458.5 eV. Nitrogen was seen on the top adherend but not the bottom adherend. Wightman (43) suggests that the nitrogen photopeak at approximately 399 eV could be due to nitride formation with titanium. Approximately 2% of aluminum was detected. No silicon was seen on any samples.

The conclusion here is that silicon observed on fracture surface of thermally aged lap shear specimens is not due to the degradation of the sized scrim cloth. The oxygen 1s photopeak of a piece of scrim cloth was found at 531.9 eV. Hence, the absence of a shift in the oxygen photopeak to a higher binding energy (approximately a 2 eV shift) further confirms the absence of scrim cloth degradation.

C. PPQ

Lead was detected on some of the Boeing fracture surfaces. In order to determine the source of lead two experiments were conducted.

A wide scan XPS spectrum of PPQ is shown in Figure 17. The XPS results for unaged and thermally aged PPQ is found in Table XVI. The elements detected include carbon, oxygen, and nitrogen. The oxgyen 1s and nitrogen 1s binding energies for both samples were very consistent at 533.6 and 399.3 eV respectively. Therefore, heating PPQ for 720 hours at 190°C in air does not cause migration of lead into the PPQ surface.

ICP (Inductively Coupled Plasma) results obtained by Ms. Varna at the Naval Air Development Center indicated the presence of 20-30 ppb of lead in a solution of PPQ, nitric acid and distilled water. A blank was run of nitric acid and distilled water. No lead was detected in the blank.

Therefore, it appears that the source of lead is PPQ and lead migrates to the adhesive-oxide interface. Hendricks et al. (32) have reported the presence of lead on samples analyzed at Boeing as well as indicating lead has little or no effect on the bond strength.

D. Pretreatments

The following sections present the results obtained from the study done on three different chemical pretreatments. XPS and SEM analysis was done to study the surface morphology and surface composition of the three different surfaces in order to determine which pretreatment offers the best surface for bonding. A fourth pair of Ti 6-4 coupons were grit blast cleaned, phosphate-fluoride pretreated and then Turco pretreated. The coupons were thermally aged for 10 and 100 hours. XPS and SEM analysis was done to observe if thermal aging affects the Turco surface and if the acidic pretreatment (phosphate-fluoride) removes residual
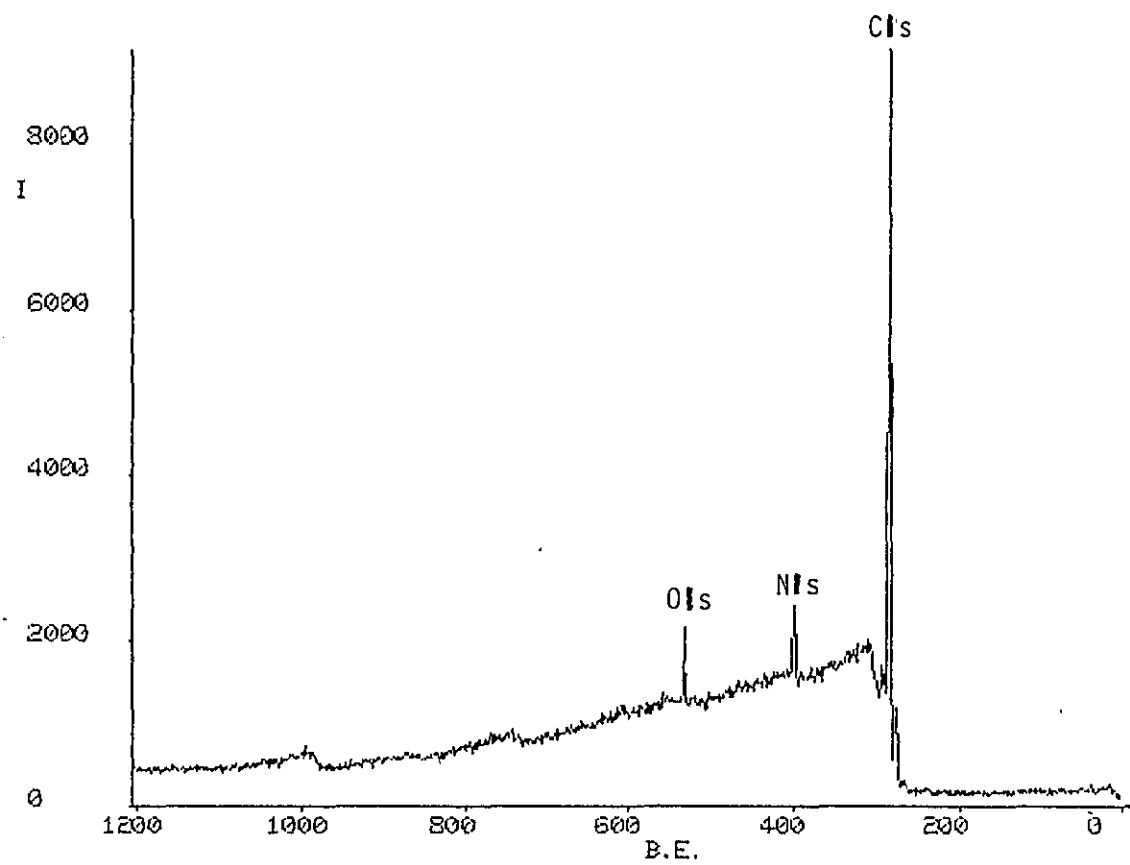
Figure 17.   XPS Wide Scan Spectrum for Thermally Aged PPQ.

TABLE XVI

XPS ANALYSIS OF UNAGED AND THERMALLY AGED PPQ

PHOTOPEAK	UNAGED		THERMALLY AGED	
	B.E.	A.F.	B.E.	A.F.
O 1s	533.6	0.049	533.9	0.067
N 1s	399.4	0.053	399.3	0.053
C 1s	285.0	0.89	285.0	0.88

sand from the grit blast cleaning process.

1. Turco:Grit Blast vs. Scotch Brite

XPS analysis of the grit blast vs. Scotch brite cleaned Turco pretreated surfaces is found in Table XVII. The adherend that was grit blast cleaned showed a small amount of silicon on the surface. A sodium 2s peak was also detected which is speculated to be a trace residual from the Turco pretreatment. A sodium 1s photopeak was detected on the Scotch Brite cleaned surface. No silicon was detected on the Scotch Brite surface. The oxygen photopeak was consistent for both adherends (528.7 eV). The titanium 2p3 photopeak was approximately 457.1 eV for both adherends. However, a lower atomic fraction for titanium was obtained on the grit blasted sample compared to the Scotch Brite sample.

The grit blast Turco surface appeared to be rougher—in texture than the Scotch Brite cleaned surface as seen in Figure 18. Therefore, the grit blast Turco pretreated surface is the candidate for bonding over the smoother Scotch Brite cleaned surface rendering a rougher surface for increased mechanical interlocking of the adhesive to the oxide.

2. Phosphate-fluoride: Grit Blast vs. Scotch Brite

XPS analysis of the pretreated adherends is found in Table XVIII. The oxygen photopeaks for both adherends were detected at approximately 530.5 eV. The titanium photopeaks for both adherends were consistent at about 459.0 eV. The oxygen and titanium binding energies for the

TABLE XVII

XPS ANALYSIS OF GRIT BLAST VS. SCOTCH BRITE CLEANED TURCO PRETREATED Ti 6-4

PHOTOPEAK	GB-T B.E.	GB-T A.F.	SB-T B.E.	SB-T A.F.
Na 1s	--	--	1073.5	0.0054
O 1s	528.7	0.28	528.8	0.30
Ti 2p3	457.1	0.075	457.2	0.050
C 1s	285.0	0.47	285.0	0.55
Si 2p	103.1	0.012	--	--
Na 2s	61.7	0.12	--	--

Figure 18. SEM Photomicrographs of Grit Blast vs. Scotch
Brite Cleaned Turco Pretreated Ti 6-4
Surfaces

TABLE XVIII

XPS ANALYSIS OF GRIT BLAST VS. SCOTCH BRITE CLEANED
PHOSPHATE FLUORIDE PRETREATED Ti 6-4

PHOTOPEAK	GB-PF		SB-PF	
	B.E.	A.F.	B.E.	A.F.
O 1s	530.5	0.34	530.8	0.34
Ti 2p3	459.0	0.10	459.3	0.10
C 1s	285.0	0.46	285.0	0.46
P 2p	-	-	133.8	0.016
Al 2p	74.3	0.035	74.5	0.019

phosphate-fluoride were slightly higher than those of the Turco pretreated surfaces. The cause for the shift is not known. Aluminum was detected on both adherends. Furthermore, a phosphorus photopeak was detected on the Scotch brite pad clean sample. A possible source of the phosphorus is a trace residual from the phosphate-fluoride pretreatment.

The SEM photomicrographs in Figure 19 of the grit blast and Scotch Brite cleaned surfaces appeared to be comparable in surface roughness. Both surfaces appeared to be relatively smooth in comparison to the Turco pretreated surfaces.

3. <u>Alkaline Peroxide:Grit Blast vs. Scotch Brite</u>

XPS analysis for the alkaline peroxide pretreated adherends cleaned using the grit blast and Scotch Brite technique is found in Table XIX. The oxygen 1s photopeaks for both adherends were consistent at 530 eV. The titanium photopeaks were consistent as well (458.5 eV). Calcium was detected on both adherends. The source of calcium is not known.

SEM analysis showed a distinct difference between the grit blast versus the Scotch Brite surface as seen in Figure 20. The grit blast surface appeared "rougher" than the Scotch Brite pad cleaned surface. The grit blast surface had a "flakier" texture than the Scotch brite pad adherend with the smoother segmented areas. Therefore, the grit blast surface would be the choice of adherend based on the surface roughness concept for bonding.

4. <u>Thermally Aged: Grit Blast-Phosphate-Fluoride Turco Pretreated Ti 6-4</u>

XPS analysis for the thermally aged grit blast cleaned, phosphate-

82
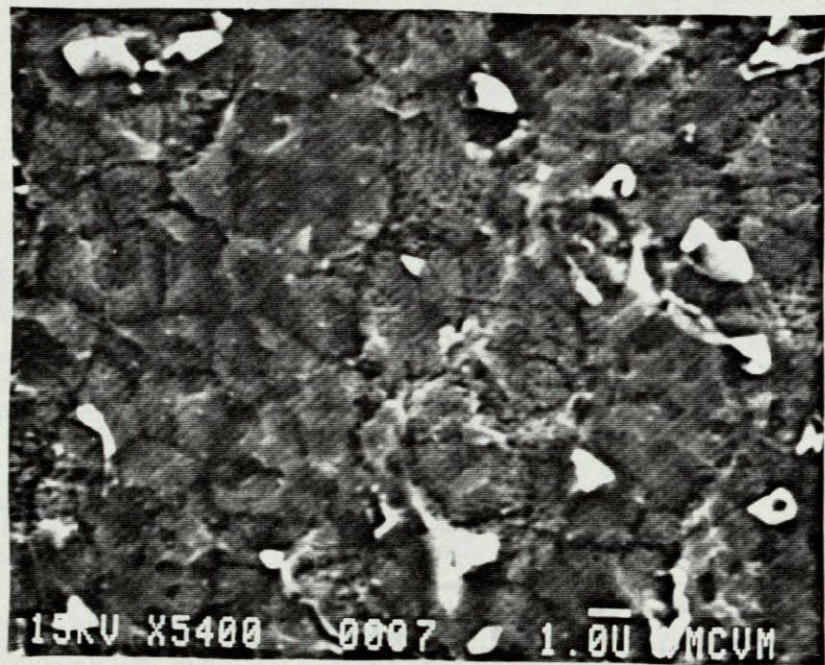
Figure 19. SEM Photomicrographs of Grit Blast vs. Scotch
Brite Cleaned Phosphate-Fluoride Pretreated
Ti 6-4 Surfaces

TABLE XIX

XPS ANALYSIS OF GRIT BLAST VS. SCOTCH BRITE CLEANED
ALKALINE PEROXIDE PRETREATED Ti 6-4

PHOTOPEAK	AP-GB		AP-SB	
	B.E.	A.F.	B.E.	A.F.
O 1s	530.8	0.35	530.0	0.36
Ti 2p3	459.0	0.11	458.5	0.080
Ca 2p	347.6	0.026	347.5	0.023
C 1s	285.0	0.45	285.0	0.47

83
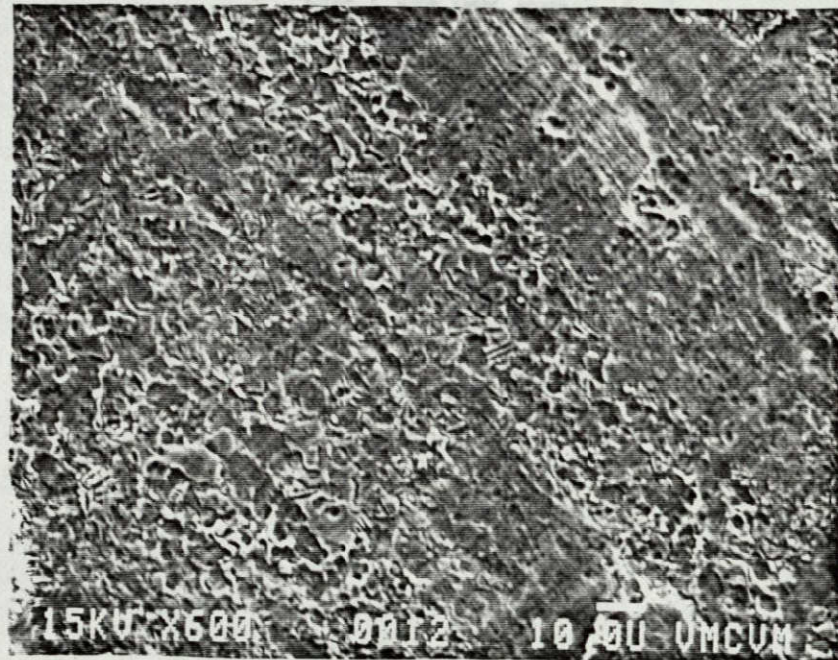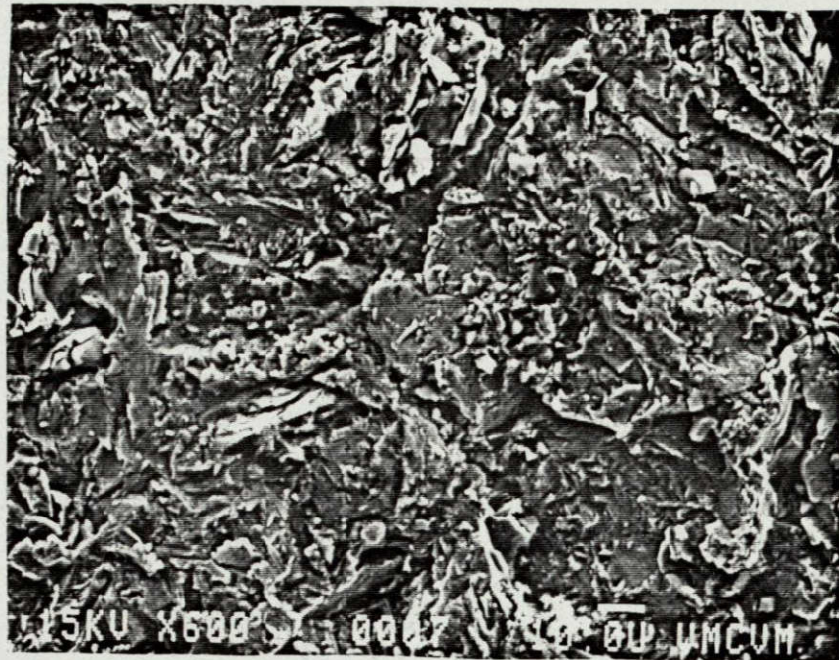
Figure 20. SEM Photomicrographs of Grit Blast vs. Scotch
Brite Cleaned Alkaline Peroxide Pretreated
Ti 6-4 Surfaces

fluoride, Turco pretreated adherend is found in Table XX. A 2.6 eV difference as seen between the 10 and 100 hours aged samples for the oxygen 1s photopeak. A 1.3 eV shift in the titanium 2p3 photopeak from 457.7 eV to 459 eV was detected. Furthermore, a nitrogen photopeak was seen on the 100 hours adherend. A possible cause for the titanium binding energy shift is the formation of titanium nitride complexes. Silicon was seen on both samples with a 1.5 eV shift as well as an increase in the atomic fraction. The detection of this silicon is a possible reason for an oxygen binding energy shift. The increase in the silicon could be due to contamination from the circulating air oven. Sulfur was seen on both adherends with a 1 eV difference. The source of sulfur is unknown. Sodium was detected on both surfaces as well. However, it is speculated that the appearance of sodium is due to trace residuals from the Turco pretreatment. Finally, the surface morphology appeared essentially the same for both the 10 and 100 hours aged samples as seen in Figure 21.

In summary, the acidic pretreatment appeared not to remove the silicon from the grit blast cleaning technique however a possible source of silicon is contamination from the circulating air oven and the thermal aging of the Turco pretreated surface doesn't affect the roughness of the surface.

E. Bonding

Two pairs of Ti 6-4 coupons were bonded with polysulfone. One pair was prepared with an acidic etch (phosphate-fluoride) while the second pair was prepared with a basic etch (Turco process). A uniform bond

TABLE XX

XPS ANALYSIS OF THERMALLY AGED GRIT BLAST CLEANED
PHOSPHATE FLUORIDE TURCO PRETREATED Ti 6-4

PHOTOPEAK	GB-PF-T(10 h)		GB-PF-T(100h)	
	B.E.	A.F.	B.E.	A.F.
O 1s	529.3	0.31	531.9	0.36
Ti 2p3	457.7	0.067	459.0	0.039
N 1s	-	-	401.7	0.01
C 1s	285.0	0.43	285.0	0.38
S 2p	167.8	0.004	168.8	0.045
Si 2p	101.1	0.0098	102.6	0.018
Na 2s	61.8	0.13	62.9	0.10

Figure 21. SEM Photomicrographs of Thermally Aged 10
and 100 Hours Grit Blast Cleaned Phosphate-
Fluoride Turco Pretreated Ti 6-4 Surfaces

line, with no gaps resulted for both bonds. No polysulfone seeped out of the bonding area of either bond.

The bonded lap shear samples were then pulled on an Instron to determine the strength of the bonds. Results indicated the stronger bond occurred with the phosphate-fluoride pretreated surface. A bond strength of 1275 psi resulted with the Turco pretreated surface whereas a bond strength of 3525 psi resulted with the phosphate-fluoride surface.

These results contradict observations of Ditchek et al. (22). Phosphate-fluoride prereated surfaces display thin oxides with little macro- or micro-roughness. Turco pretreated surfaces have a high degree of macro-roughness as well as a thin oxide. Hence, according to Ditchek et al. (22), the rougher the surface the stronger the bond. Therefore, the Turco treated surface should have given the stronger bond. Possible explanations for a weaker Turco bond include: (i) the Turco bath, (ii) hot rinse cycle resulting in residual contaminants from the etching process, (iii) the hot air drying, or (iv) silicon contamination from the grit blast cleaning.

XPS analysis of the Turco pretreated, polysulfone bonded Ti 6-4 indicates interfacial failure supported by the absence of a titanium photopeak on the adhesive failure surface (see Table XXI). Residual sodium was detected on both failure surfaces with approximately 4% of sodium on the metal failure and 1% on the adhesive failure. A larger percentage of sodium is expected on the metal failure surface due to the Turco surface pretreatment. The oxygen 1s binding energy on the MFS was

C-2

TABLE XXI

XPS ANALYSIS OF TURCO-POLYSULFONE BONDED Ti 6-4

PHOTOPEAK	MFS		AFS	
	B.E.	A.F.	B.E.	A.F.
Na 1s	1070.8	0.041	1071.0	0.0099
O 1s	529.8	0.27	532.5	0.15
Ti 2p3	458.4	0.032	NSP	
C 1s	285.0	0.64	285.0	0.80
S 2p	168.0	0.014	167.5	0.022
Si 2p			102.2	0.015

approximately 530 eV indicative of the metal oxide. The oxygen 1s

binding energy on the AFS was 532.5 eV indicative of the polymer,

polysulfone. Siochi (53) found the oxygen 1s photopeak of polysulfone

to be approximately 533 eV. Sulfur was detected on both failure

surfaces which is indicative of the presence of polysulfone. The

appearance of sulfur on the metal failure surface indicates a polymer

coating on the MFS however not greater than 5 nm in thickness. A trace

amount of silicon was detected on the AFS.

Finally, the phosphate-fluoride pretreated surface appeared to have

failed in the mixed mode. However, the bond did not fully break and the

adhesive kept stretching. Therefore, according to the results obtained,

the grit blast phosphate-fluoride pretreated surface gives the best

surface for bonding with polysulfone when comparing Turco to phosphate-

fluoride processes.

CHAPTER V

SUMMARY

The emphasis on the present research has focused on the surface analysis of the interphase in fractured lap shear Ti 6-4 adherends bonded with polyphenylquinoxaline (PPQ) and polysulfone (PS). The effects of adherend pretreatment, stress level, thermal aging, anodizing voltage, and modified adhesive on lap shear strength were investigated for the PPQ samples. The effect of adherend pretreatment on lap shear strength were investigated for the PS samples.

Cohesive failure was associated with the absence of a Ti 2p3 XPS photopeak on the fracture surface whereas the presence of this peak was evidence of interfacial failure at the 5 nm level. Furthermore, high lap shear strengths were also associated with cohesive failure. The modification of the PPQ with boron powder showed reduced lap shear strengths in Ti 6-4 adherends bonded with modified adhesive. The aging time showed an inverse effect on the lap shear strengths of PPQ samples. That is, as the aging time increased the lap shear strength decreased. Variation in the stress level on samples aged at 232°C for 1000 hours had little or no effect on lap shear samples pretreated using chromic acid anodization, bonded with PPQ and tested at 18°C. Furthermore, chromic acid anodization at 10V gave superior lap shear strengths to those obtained with 5V anodization.

Lead and silicon were detected on some of the PPQ fracture surfaces. Therefore, subsequent experiments were designed to determine the sources of lead and silicon on the fractured lap shear samples. The

92

source of lead is the PPQ and lead migrates to the adhesive-oxide interface. The source of silicon is not from the degradation of the sized scrim cloth used in the bonding process.

Three different chemical pretreatments were done to determine which pretreatment offers the roughest surface for bonding Ti 6-4 with polysulfone (PS). The Turco pretreated Ti 6-4 surface appeared to give the optimum surface for bonding in comparison to alkaline peroxide and phosphate-fluoride treated surfaces. When a Turco pretreated surface which had been grit blasted and phosphate-fluoride pretreated prior to the Turco preteatment was thermally aged for 10 and 100 hours, no changes were seen in the surface topography. It can be concluded that the thermal aging appears not to affect the roughness of the Turco pretreated surface.

Ti 6-4 adherends were pretreated using the Turco and phosphate-fluoride processes, bonded with polysulfone and then fractured. Polysulfone offered bonding advantages over PPQ. The phosphate-fluoride pretreated Ti 6-4 gave a higher lap shear strength than the Turco pretreated surface bonded in the same manner. This result was opposite to that expected based on the concept of surface roughness.

VI. ACKNOWLEDGEMENT

Appreciation is given to Don Progar at the NASA Langley Research Center, Dr. Carl Hendricks at the Boeing Aerospace Company, Jean Ann Skiles, Sandy Gay, Mia Siochi, Margaret Green, and Kim Newcomb at Virginia Tech for technical assistance. Also, a special appreciation to Frank Cromer and Steve McCartney for running the XPS spectra.

VII. REFERENCES

1. A. A. Roche, J. S. Solomon, and W. L. Baun, Appl. Surf. Sci., 1, 83(1981).

2. M. Natan and J. D. Venables, J. Adhesion, 15, 125-136 (1983).

3. A. J. Kinloch, J. Adhesion, 10, 193-219 (1979).

4. W. Chen, R. Siriwardane, J. P. Wightman, 12th National SAMPE Technical Conference, Oct. (1980).

5. P. M. Hergenrother and D. J. Progar, Adhesives Age, 38-43 Dec. (1977).

6. W. E. Driver, Plastics Chemistry and Technology, (Van Nostrand Reinhold Company, New York, 1979), p. 18.

7. S. S. Schwartz and S. H. Goodman, Plastics Materials and Processes, (Van Nostrand Reinhold Company, New York, 1982), pp. 270-280.

8. G. L. Schneberger, Adhesives Age, 42-46, Jan. 1980.

9. J. R. Huntsberger, J. Adhesion, 12, 3-12 (1981).

10. F. P. Bowden and W. R. Throssel, Nature, 167, 601 (1957).

11. N. J. De Lollis, Handbook of Adhesive Bonding (McGraw-Hill, New York, 1973), Ed. Charles V. Cagle, Chap. 2, pp. 2-1-2-16.

12. I. C. Sanchez, Polymer Engineer and Sci., 24, 2, 79-86 (1984).

13. Proceedings of the Workshop on Reliability of Adhesive Bonds Under Severe Environment. National Materials Advisory Board-Division of Engineering-National Research Council, NMAB-XXX, National Academy of Sciences-National Academy of Engineering. Washington, May, 1984.

14. J. C. Bittence, ME, 41-43, July (1983).

15. T. A. Bush, M. E. Counts, J. P. Wightman, Adhesion Science and Technology, (Plenum, New York, 1975), Ed. Lieng Huang Lee, Vol. 9A, pp. 365-392.

16. D. E. Packham, Adhesion Aspects of Polymeric Coatings, (Plenum, New York, 1983), Ed. K. L. Mittal, pp. 19-44.

17. K. W. Allen and H. S. Alsalim, J. Adhesion, 6, 229-237 (1974).

TA4

93

18. K. W. Allen, H. S. Alsalim, and W. C. Wake, J. Adhesion, 6 153-164 (1974).

19. R. Rerrier, J. J. Bodu, and M. Brunin, Surface Techn., 8, 463 (1979).

20. W. Chen, D. W. Dwight, W. R. Kiang, and J. P. Wightman in Surface Contamination, (Plenum, New York, 1979), Ed. K. L. Mittal, Vol. 2, p. 655.

21. B. M. Ditchek, K. R. Breen, T. S. Sun, J. D. Venables, and S. R. Brown, 12th National SAMPE Tech. Conf., Oct. (1980).

22. D. M. Ditchek, K. R. Breen, T. S. Sun and J. D. Venables, 25th National SAMPE Symp. and Exhib., 25 (1980).

23. M. Natan, J. D. Venables, and K. R. Breen, 27th National SAMPE Symp. 178 (1982).

24. A. Matthews, Am. Mineral, 61, 419-424 (1976).

25. J. M. Chen, T. S. Sun, and J. D. Venables, 22nd National SAMPE Symp. and Exhib., 25 April (1977).

26. J. C. Mason, R. Siriwardane, and J. P. Wightman, J. Adhesion, 11, 315-328 (1981).

27. F. M. Fowkes, J. Adhesion, 4, 155 (1972).

28. H. R. Anderson, Jr., F. M. Fowkes, and F. H. Hielscher, J. Polymer Sci., Polymer Phys. Ed., 14, 879 (1976).

29. H. R. Anderson Jr. and J. D. Swalen, J. Adhesion, 9, 197 (1978).

30. F. M. Fowkes, Organic Coatings and Plastic Chemistry Preprints, 40, 13 (1979).

31. K. Tanabe, Solid Acids and Bases (Academic Press, New York, 1970).

32. S. G. Hill, P. D. Peters, and C. L. Hendricks, Boeing-Evaluation of High Temperature Structural Adhesives for Extended Service, NAS1-15605, NASA-Langley, Hampton, VA, July 1982.

33. P. M. Hergenrother, Polym. Engineer and Sci., 21, No. 16, 1072-1078 (1981).

34. P. M. Hergenrother, Macromolecules, 14, 898-904 (1981).

35. A. K. St. Clair and T. L. St. Clair, SAMPE Quarterly, 13, No. 1, 20-25 (1981).

36. T. L. St. Clair and D. J. Progar, ACS Polymer Preprints, 16, No. 1
    538 (1975).

37. D. J. Progar and T. L. St. Clair, Preprints, 7th National SAMPE
    Tech. Conf., 7, 53 (1975).

38. A. K. St. Clair, W. S. Slemp., and T. L. St. Clair, Adhesives Age,
    22, 35 (1979).

39. A. F. Lewis and R. T. Natarajan, Polymer Sci. and Techn., 9A, L. H.
    Lee, Ed. (Plenum Press, New York, 1975). pp. 563-577.

40. M. Natan, K. R. Breen, and J. D. Venables, MMLTR 81-42(c),
    Martin Marietta, Sept. 1981.

41. J. W. Shultze, U. Stimming, and J. Werze, B. Bunsenges, Phys.
    Chem., 86, 2176 (1982).

42. D. W. Dwight, M. E. Counts, and J. P. Wightman, in Colloid and
    Interface Science, Wetting, Surface Tension, and Water (Academic
    Press, New York, 1976).

43. J. P. Wightman, SAMPE Quarterly, 13, No. 1, 1 (1981).

44. C. L. Hendricks, Evaluation of Higher Temperature Structural
    Adhesives for Extended Service, First Semi Annual Progress Report
    NAS1-15605, NASA-Langley, Hampton, VA, June 1979.

45. C. L. Hendricks, Evaluation of High Temperature Structural
    Adhesives for Extended Use, Bimonthly Technical Report NAS1-15605,
    NASA-Langley, Hampton, VA, July 1979.

46. A. L. Baun, J. Adhesion, 12, 81-98 (1981).

47. S. Brown, Naval Air Development Center.

48. S. Dias and J. P. Wightman in Adhesive Chemistry-Recent Trends and
    Developments, Ed. L. H. Lee (Plenum, New York) in Press.

49. J. Jen, Unpublished results (1983).

50. T. L. Egerton, Y. Kang, G. D. Parfitt, and J. P. Wightman, Colloids
    and Surfaces, 7, 311 (1983).

51. J. A. Filbey, Unpublished Results (1984).

52. M. J. Mandry and G. Rosenblatt, J. Electro. Soc., 29 (1972).

53. E. J. Siochi, Unpublished Results (1984).